AGU PUBLICATIONS

JGR

Journal of Geophysical Research: Atmospheres

RESEARCH ARTICLE

10.1002/2013JD021218

Key Points:
- We seek to improve the aerosol activation behavior in kilometer-scale models
- A method to constrain the subgrid-scale updraft velocity is presented
- We highlight the potential implication for aerosol-cloud interactions modeling

Correspondence to:
F. F. Malavelle,
f.malavelle@exeter.ac.uk

Citation:
Malavelle, F. F., J. M. Haywood, P. R. Field, A. A. Hill, S. J. Abel, A. P. Lock, B. J. Shipway, and K. McBeath (2014), A method to represent subgrid-scale updraft velocity in kilometer-scale models: Implication for aerosol activation, *J. Geophys. Res. Atmos.*, *119*, 4149–4173, doi:10.1002/2013JD021218.

Received 18 NOV 2013
Accepted 17 MAR 2014
Accepted article online 19 MAR 2014
Published online 9 APR 2014

A method to represent subgrid-scale updraft velocity in kilometer-scale models: Implication for aerosol activation

Florent F. Malavelle[1], Jim M. Haywood[1,2], Paul R. Field[2,3], Adrian A. Hill[2], Steven J. Abel[2], Adrian P. Lock[2], Ben J. Shipway[2], and Kirsty McBeath[2]

[1]College of Engineering Mathematics and Physical Sciences, University of Exeter, Exeter, UK, [2]Met Office, Exeter, UK, [3]School of Earth and Environment, University of Leeds, Leeds, UK

Abstract Updraft velocities strongly control the activation of aerosol particles or that component that act as cloud condensation nuclei (CCN). For kilometer-scale models, vertical motions are partially resolved but the subgrid-scale (SGS) contribution needs to be parametrized or constrained to properly represent the activation of CCNs. This study presents a method to estimate the missing SGS (or unresolved) contribution to vertical velocity variability in models with horizontal grid sizes up to ~2 km. A framework based on Large Eddy Simulations (LES) and high-resolution aircraft observations of stratocumulus and shallow cumulus clouds has been developed and applied to output from the United Kingdom Met Office Unified Model (UM) operating at kilometer-scale resolutions in numerical weather prediction configuration. For a stratocumulus deck simulation, we show that the UM 1 km model underestimates significantly the variability of updraft velocity with an averaged cloud base standard deviation between 0.04 and 0.05 m s^{-1} compared to LES and aircraft estimates of 0.38 and 0.54 m s^{-1}, respectively. Once the SGS variability is considered, the UM corrected averages are between 0.34 and 0.44 m s^{-1}. Off-line calculations of CCN-activated fraction using an activation scheme have been performed to illustrate the implication of including the SGS vertical velocity. It suggests increased CCN-activated fraction from 0.52 to 0.89 (respectively, 0.10 to 0.54) for a clean (respectively, polluted) aerosol environment for simulations with a 1 km horizontal grid size. Our results highlight the importance of representing the SGS vertical velocity in kilometer-scale simulations of aerosol-cloud interactions.

1. Introduction

Aerosol-Cloud interactions (ACI) are complex because they span a large range of spatial and temporal scales. Despite recent improvements in the parametrizations of ACI in Global Circulation Models (GCM) and Earth System Models which has seen a move from empirical to more mechanistic approaches [e.g., *Ming et al.*, 2007; *Wang et al.*, 2011; *Tonttila et al.*, 2013; *West et al.*, 2013], impacts on climate remain poorly understood and constrained, hence highly uncertain [*Lohmann and Feichter*, 2005; *Forster et al.*, 2007]. The coarse spatial and temporal resolution used in GCMs is unable to resolve the fine-scale processes (e.g., vertical velocity and turbulent mixing) or the microphysical and dynamic feedbacks that are important in ACI [*Stevens and Boucher*, 2012; *Seifert et al.*, 2012], which leads to this uncertainty. As a result, in situ observations and process modeling studies are invaluable in understanding ACI and their implication for climate [*Stevens and Feingold*, 2009].

High-resolution atmospheric models such as cloud-resolving models (CRM) and Large Eddy Simulation models (LES) are among the most powerful numerical tools available to investigate ACI as they can explicitly resolve individual clouds, the small-scale dynamics and subsequent feedbacks [e.g., *Ackerman et al.*, 2004; *Jiang and Feingold*, 2006; *Xue and Feingold*, 2006; *Sandu et al.*, 2008; *Hill et al.*, 2008; *Grabowski and Morrison*, 2011]. However, due to their computational cost, simulation domains are restricted to small areas, typically $\mathcal{O}(10^2\ km^2)$, and short periods of about 1 or 2 days. This limits the potential for CRMs and LES for investigating large-scale feedbacks and buffering effects [*de Roode et al.*, 2004; *Stevens and Feingold*, 2009; *Koren and Feingold*, 2011; *Seifert et al.*, 2012] and means that extrapolating to global scale, where such effects are important, is nontrivial [*Stevens and Boucher*, 2012].

In order to bridge the gap between the cloud scale and the global scale, a possible approach is using high-resolution large-scale models such as those from operational numerical weather prediction (NWP)

[*Tonttila et al.*, 2011; *Kocha et al.*, 2012; *Seifert et al.*, 2012]. NWP models are now running at operational resolutions of a few kilometers offering new capability in terms of resolving the atmospheric structures (e.g., explicit rather than parametrized convection). Such models can incorporate complex microphysical representations of ACI over sufficiently large areas and for long enough periods to investigate the couplings between clouds and their environment. This study presents an approach to improve the microphysical link between aerosols and clouds in such a model, namely, the United Kingdom Met Office Unified Model operating at kilometer-scale resolution [*Brown et al.*, 2012], which can be applied to other mesoscale models with equivalent grid resolution. More specifically, this work focuses on the parametrization of the subgrid-scale vertical velocity (w) and aerosol activation.

The microphysical link between aerosols and clouds come through the process of droplet activation which is a strong function of the cloud-scale updraft velocity. A positive vertical velocity will lead to an adiabatic cooling associated with an increase in relative humidity. If the relative humidity exceeds 100%, i.e., the parcel is supersaturated, aerosol particles (termed cloud condensation nuclei; CCN) can activate and grow to form cloud droplets [*Twomey*, 1959; *Pruppacher and Klett*, 1997]. Physically based parametrizations that predict number of activated CCN as a function of aerosol properties (size, number, and composition) and vertical velocity have been developed and implemented in GCMs [*Ghan et al.*, 2011]. These parametrizations are sensitive to updraft velocity which poses a problem because the subcloud velocity which controls activation occurs at smaller scales than the grid of models, even for NWP models running with a horizontal grid spacing $\mathcal{O}(1km)$. In fact, a kilometer-scale model may resolve some aggregation of convective cells but no individual cells, which may lead to the erroneous perception that these ranges of resolution are suitable for realistically representing ACI. *Tonttila et al.* [2011] showed for instance that the nonhydrostatic mesoscale model AROME running with a 2.5 km horizontal grid produces a standard deviation of vertical velocity that is 4 to 8 times smaller than that observed using CLOUDNET remote-sensing network. Adding a term proportional to the Turbulent Kinetic Energy (TKE) on the resolved grid point vertical velocity compensates for some of the underestimation. The study by *Tonttila et al.* [2011] illustrates that a prerequisite for a more robust representation of ACI in kilometer-scale NWP models is a constraint on the subgrid-scale (SGS) variability of updraft velocity.

The treatment of the SGS vertical velocity applied to the activation problem in large-scale models is traditionally handled by one of two distinct approaches: the *probability density function (pdf) approach* or the *characteristic approach* [*Golaz et al.*, 2011; *West et al.*, 2013]. In the pdf approach a vertical velocity probability density function (pdf) is assumed within the model grid box [*Ghan et al.*, 1997]. The grid-averaged number of activated aerosols can be derived by integrating the local activation parametrization over the pdf of w. The main challenges consist of assessing the moments and the shape of the distribution. In practice, these are not well understood and hence difficult to parametrize. The simplest assumption is to prescribe the pdf using observational data or CRM simulations for specific cloud regimes. However, finding universal pdfs is difficult as the properties of the distribution vary significantly between cloud regimes and are dependent on cloud height, boundary layer type, phase of diurnal cycle, or latent heat exchange (e.g., drizzle/rain) among other factors [*Zhu and Zuidema*, 2009; *Hogan et al.*, 2009; *Bretherton et al.*, 2010]. Current state of the art GCMs and large-scale models generally assume that the subgrid variability in w follows a single-Gaussian distribution of probabilities across the grid box and that all subgrid variability is due to turbulence [*Ghan et al.*, 1997]. The standard deviation (σ_w) of the distribution is typically parameterized using large-scale diagnostics such as TKE (if predicted by the host model), or K, the eddy diffusivity. These distributions may be suitable for stratocumulus clouds but do not represent shallow cumulus convection well as they are unskewed. *Larson et al.* [2002] showed for instance that a double-Gaussian pdf provides a better representation of SGS variability in boundary layer clouds. A turbulence cloud scheme based on such pdf has been developed [*Golaz et al.*, 2002; *Zhu and Zhao*, 2008] and prognoses joint pdfs of vertical velocity, temperature, and moisture which serve as a condensation scheme and a turbulence closure for boundary layer clouds. *Guo et al.* [2010] recently extended this approach to predict cloud droplet number in the single-column version of the Geophysical Fluid Dynamics Laboratory GCM, but this has yet to be implemented in a 3-D large-scale model. Indeed, the computational cost of such scheme is significant because of the higher-order turbulence closure needed to fully specify the pdf.

In the characteristic approach it is assumed that a characteristic single updraft velocity, w^*, can be used to compute a representative number of activated CCN. The motivation is the reduction in the computational expense compared to an integration over a pdf. The characteristic velocity is usually diagnosed as the sum

of the grid box resolved updraft velocity and a term proportional to σ_w. As in the pdf approach, the latter is generally related to TKE or K, times an empirical factor which is sometime derived assuming TKE isotropy [e.g., *Lohmann et al.*, 1999; *Morrison and Pinto*, 2005; *Morrison and Gettelman*, 2008; *Tonttila et al.*, 2011]. The general applicability of the characteristic approach is far from being established as it may underestimate the potential effect of the nonlinear relation between w and the number of activated CCN [*West et al.*, 2013]. As a result, this concept has been recently revisited by *Morales and Nenes* [2010] for stratocumulus clouds. The authors defined w^* as the value for which the number of activated aerosols equals the value averaged over the pdf of w. It is given as $w^* = \lambda^* \times \sigma_w$ where λ^* is an analytical expression function of the CCN spectrum steepness.

In both the pdf approach and characteristic approach, the grid box variability in vertical velocity needs to be evaluated. Here we do not seek to compare the two approaches; instead, we focus our effort on finding predictors to diagnose σ_w. The aim of this study is to develop a computationally efficient method which should satisfy the efficiency requirement of NWP, to estimate the missing SGS (or unresolved) contribution to vertical velocity variability in models with kilometer-scale grid resolution or less. Once, the SGS term is constrained, the total vertical velocity variability can be used to accurately represent the activation of CCNs using either a pdf approach or characteristic approach. Details of the method are described in the remainder of the paper which is structured as follows: In section 2 we present the strategy adopted to develop a method to estimate the SGS updraft velocity variability in kilometer-scale models. Section 3 describes the modeling tools and observational data set used in this study. Formulation of the method and underlying assumptions are detailed throughout section 4. In section 5 we present the results of the method applied to the Unified Model outputs. Implication for CCN activation are explored in section 6. Concluding remarks and outlooks are finally summarized in section 7.

2. Problematic and Strategy

Large-scale models, even with kilometer-scale resolution, have problems with reproducing the correct activation behavior due the underestimation of the vertical velocity [e.g., *Ivanova and Leighton*, 2008]. As discussed above, a pdf approach or a characteristic approach can be used to circumvent the problem. In either of these approaches, it is generally assumed that all the subgrid variability is due to turbulence [*Ghan et al.*, 1997]. While relying on a turbulence parametrization to diagnose the SGS updraft velocity variability has a sound physical basis, NWP and research mesoscale models with horizontal resolutions $\mathcal{O}$(0.5–2km) operate in the so-called *grey zone* or *terra incognita* [*Wyngaard*, 2004; *Honnert et al.*, 2011; *Dorrestijn et al.*, 2013]. Such resolution is too low to resolve the turbulent eddies explicitly, but too high to rely on deterministic parametrizations based on quasi-equilibrium assumptions [*Dorrestijn et al.*, 2013]. This challenges current parametrizations and their skills remain uncertain at these resolutions [*Honnert et al.*, 2011]. Hence, we want to develop a parameterization for the vertical velocity variability that (i) does not rely on a TKE diagnostic because it is not always diagnosed when the convection parametrization is handling the vertical mixing, and (ii) does not a rely on a high-order turbulence scheme because of the grey zone issues and computational costs associated with NWP application.

Models with kilometer resolution partially resolve the vertical motions (Figure 1). We propose to take advantage of this resolved information to constrain the subgrid variations in vertical velocity. The issue is to assess how much variability can be resolved and how much is subgrid at a kilometer-scale resolution. To tackle this problem, we will first derive a function (the "partition function" hereafter) that separates the total updraft vertical velocity variance into its subgrid and resolved contributions at a given resolution. This partition function will allow us to estimate the missing subgrid contribution to the vertical velocity variability in the kilometer-scale model.

To construct the partition function, we will apply a coarse-graining procedure (section 4.1) to high-resolution aircraft observations and LES. The aim of the coarse graining is to use a sufficiently high-resolution data set that captures the total vertical velocity variability, and perform successive horizontal spatial means of the resulting fields up to a grid resolution typical of a kilometer-scale model, to then quantify the contribution of the resolved and subgrid terms. This approach follows the work of *Honnert et al.* [2011], but we extend the concept to vertical velocity variances and will focus on two types of moist boundary layers which have important implications for climate, namely, trade wind cumulus and marine stratocumulus-topped boundary layers.

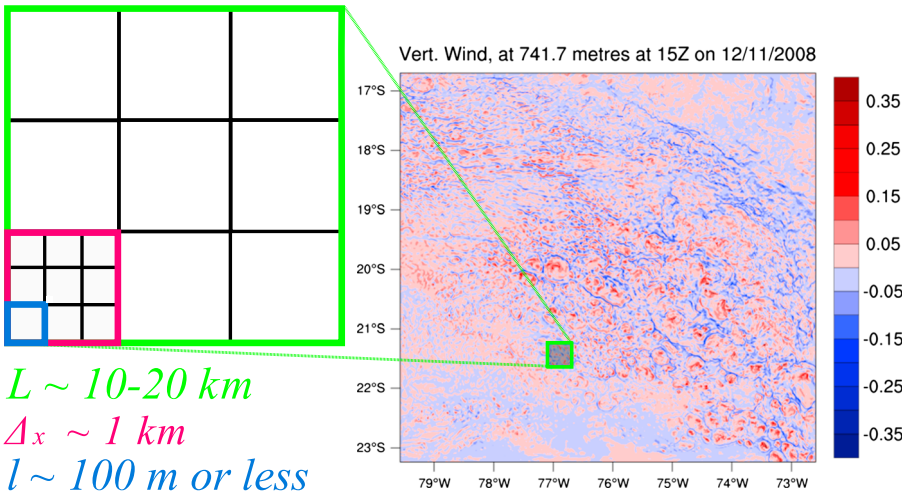

Figure 1. (left) A depiction of the three length scales discussed in section 4.1. *L* is the horizontal length for the entire LES domain. At the length scale *l* of the LES model resolution, cloud-scale processes are explicitly resolved. Length scale Δ_x lies in between *L* and *l* and can be seen as a length scale typical of a kilometer-scale model for which we need to evaluate the subgrid/resolved partition of vertical velocity variability. (right) Example of vertical velocity (units are m s^{-1}) from a Unified Model forecast on a 750 × 750 km^2 domain at 1 km horizontal resolution centered on a stratocumulus deck in the southeast Pacific (VAMOS Ocean Cloud Atmosphere Land Study (VOCALS) domain).

In summary, the turbulent variations in vertical velocity are extracted from vertical velocity resolved in kilometer-scale simulations using the following "bootstrapping" approach:

1. A priori construction of a scale-linking partition function of vertical velocity variability using a coarse-graining procedure on high-resolution aircraft observations and LES.
2. In the kilometer-scale model, diagnosis of the ratio of resolved to total vertical velocity variability at the model resolution using the prescribed partition function.
3. In parallel, estimation of the resolved vertical velocity variability in the kilometer-scale model.
4. Ultimately, parameterization of the subgrid vertical velocity variability term as a function of the resolved term and the ratio of resolved over total vertical velocity variability.

Once the subgrid term is constrained and added to the resolved term, it provides an estimate of the total vertical velocity variability that can be used in either a pdf approach or a characteristic approach to calculate CCN activation. This final point is not covered exhaustively in this study as full integration of the framework in the Unified Model is still ongoing. However, we will present off-line calculations with an activation scheme to illustrate potential implications of neglecting the SGS velocities in kilometer-scale simulations (section 6).

To develop and test the method to be described, a combination of two models and aircraft observation is considered. The first model is the United Kingdom Met Office Large Eddy Model (LEM hereafter) [*Petch*, 2006, and references therein] which is a LES model that resolves the fine structures of vertical motion. It is used as estimate of reality to produce the high-resolution fields of vertical velocity. The LEM is run for two cases that covers the most frequent type of marine boundary layer clouds: the Atlantic Stratocumulus to Cumulus Transition Experiment (ASTEX) [*Albrecht et al.*, 1995] and the Rain In Cumulus over the Ocean experiment (RICO) [*Rauber et al.*, 2007]. These simulations are used to construct the partition function. In parallel, high-resolution aircraft observations collected during the VAMOS Ocean Cloud Atmosphere Land Study-Regional Experiment (VOCALS-REx) [*Wood et al.*, 2011]) are also considered to construct the partition function. The second model is the United Kingdom Met Office Unified Model (UM hereafter). The UM can be used for a wide range of applications from weather to climate prediction. In limited area NWP configuration, it is used with grid resolutions varying from 1.5 km for operational forecasts over the UK, to a few hundred meters in research mode. Here it is used as a large-scale model to produce forecasts at kilometer-scale resolutions. The UM is first run to simulate a stratocumulus deck over the southeast Pacific (VOCALS-REX region). Second, it is use to simulate a cold air outbreak in the North Atlantic (CONSTRAIN experiment) [*Field et al.*, 2013]. Although the CONSTRAIN simulations involve a more complex cloud microphysics (e.g., the presence of mixed-phase clouds) than in the cases used to construct the partition function, testing our developments

on this case is an attempt to challenge the robustness of the method for a different large-scale environment. Our method is applied off line to the UM forecasts and the results will be compared with idealized LEM simulations of VOCALS-REx and CONSTRAIN and with the aircraft observations from VOCALS-REx as well (section 5).

3. Model Configurations and Observations

3.1. Large Eddy Simulations and Observations

Hereafter, we will be referring to four boundary layer (BL) regimes that characterize the BL observed in the four case study aforementioned:(1) *M-STBL:* well-mixed stratocumulus-topped BL; (2) *D-STBL:* decoupled stratocumulus-topped BL; (3) *C-STBL:* cumulus under stratocumulus-topped BL; and (4) *CBL:* cumulus-capped BL.

3.1.1. LEM-ASTEX

The ASTEX campaign was conducted in June 1992 in the northeast Atlantic near the Azores (approx 37°N, 25°W) with the goal to study the climatologically important transition between solid stratocumulus and subtropical trade cumulus cloud regimes [*Albrecht et al.*, 1995]. The LEM is used to simulate a shallow drizzling stratocumulus-capped marine boundary layer that deepens after 2 days supporting trade wind cumulus detraining into a patchy and fairly thin upper stratocumulus layer (LEM-ASTEX simulation). Model setup follows the GEWEX cloud system study ASTEX modeling intercomparison recommendation fully described in *van der Dussen et al.* [2013]. The domain of the simulation extends over a 640 × 320 horizontal grid with resolution of 35 m (22.4 × 11.2 km). The vertical resolution is 15 m below an altitude of 540 m. It is increased to 5 m between 540 and 1760 m and then decreases exponentially above this level. The model runs for 42 h from 1600 UTC on 12 June 1992. Note that the last 10 h of the simulations are less reliable (sponge layer, coarser vertical resolution, appropriate subsidence is highly uncertain); hence, we will not consider the CBL regime at the end of the simulation. We use the instantaneous hourly outputs from $T_0 + 4$h to $T_0 + 34$h. We separate the results into M-STBL ($T_0 + 4\text{h} \rightarrow T_0 + 10\text{h}$), D-STBL ($T_0 + 12\text{h} \rightarrow T_0 + 28\text{h}$) and C-STBL ($T_0 + 30\text{h} \rightarrow T_0 + 34\text{h}$). A similar metric for decoupling as defined in *Jones et al.* [2011] based on the difference of the total water content (Δq_t) between the bottom 25% and the top 75% of the boundary layer is used to identify when it begins to decouple (see Figures 3b and 3d).

3.1.2. LEM-RICO

The RICO campaign objectives were to evaluate precipitation in association with shallow cumulus across a broad range of scales. The experiment took place during November 2004 and January 2005 off the Caribbean islands of Antigua and Barbuda (approximately 17°N, 62°W) within the northeast trades of the western Atlantic [*Rauber et al.*, 2007]. The LEM was initialized with profiles from 19 January 2005 to simulate shallow convection in the marine boundary layer where fairly deep (and narrow) warm cumulus fields develop (LEM-RICO simulation). The domain of the simulation extends over a 256 × 256 horizontal grid with a resolution of 100 m (25.6 × 25.6 km). The vertical domain consists of 100 layers on a stretched grid using spacing varying from 40 m in the boundary layer, increasing to 100 m in the midtroposphere up to 7 km and then further degraded to 200 m toward the top of the domain at 10 km. We use the same microphysical setup as the experiment "UPLINGER-2M-N-HR" described in *Abel and Shipway* [2007]. The simulation reaches a quasi-equilibrium state after approximately 10–12 h, while the instantaneous hourly outputs used here are taken from hours 24 to 36.

3.1.3. LEM-VOCALS and OBS-VOCALS

VOCALS-REx was an international field program conducted between October and November 2008. It was designed to make observations of poorly understood but critical components of the coupled climate system of the southeast Pacific. This region is characterized by strong coastal upwelling, the coolest sea surface temperatures (SSTs) in the tropical belt, and is home to the largest subtropical stratocumulus deck on earth. We use the in-cloud data set of winds/turbulence and Liquid Water Content (LWC) from both the NSF/NCAR Lockheed C-130 aircraft (25 Hz sampling rate, i.e., approximately 4 m resolution) and the FAAM BAe-146 aircraft (32 Hz sampling rate, i.e., approximately 3.4 m resolution) to analyze the variability of vertical velocity in well-mixed and slightly decoupled stratocumulus-topped boundary layers (OBS-VOCALS, hereafter). We have selected legs that present a fairly constant LWC to avoid complex break up situations. We also avoid including in our statistics the variances at the top of the cloud layers influenced by turbulent entrainment which is less relevant for the activation processes. This was achieved by retaining only legs at altitudes within the lowest third of the cloud depth. The same coarse-graining procedure applied to the 3-D LEM

outputs described in section 4.1 is performed on each individual leg but on a 1-D horizontal level. To calculate the depth of the boundary layer we used the nearby legs to identify when the aircraft enters and exits the cloud. We have then assumed that the boundary layer and the cloud tops coincide. The latter is identified based on a LWC threshold and a visual verification of the LWC profiles, aircraft altitude, and wind measurements. To ensure that the sample size of each in-cloud leg was large enough to capture all of the w variability, we did not retain legs for which the length of continuous measurements was shorter than approximately 20 km. We found that subsampled legs greater than 10 km usually capture all of the variability of the whole legs (not shown). Applying these criteria leave about 55 remaining in-cloud leg samples within the campaign period to compute coarse-grained fields of vertical velocity. Finally, prior to coarse graining the data set, the vertical velocity data were linearly detrended to remove potential drift in the instrumentation. We also removed potential mesoscale fluctuations in w (e.g., gravity waves) by not including wavelengths larger than 10 km from the power spectrum of vertical velocity and computing back the inversed Fourier transform of the filtered power spectrum. This contribution remains small, and we assume that it is not relevant at the scale of activation processes.

In addition, the LEM has been used to produce a 46 h simulation of a stratocumulus deck based on idealized profiles from the VOCALS campaign (LEM-VOCALS simulation). The LEM simulates a 100% cloud cover stratocumulus deck which clears and breaks up toward the end of the simulation. The horizontal grid is 514 by 514 points with a resolution of 120 m and the vertical resolution is 20 m below the inversion (105 vertical levels between 0 and 2000 m). The model is initialized from 07:00 UTC (approximately 02:00 local solar time) and the outputs analyzed are taken during the period $T_0 + 10$ h to $T_0 + 16$ h while the cloud cover remains 100%. The updraft velocity standard deviations, σ_w, from the LEM-VOCALS run have been reinterpolated on a 1 by 1 km resolution grid similar as the UM grid prior to computing the histograms of σ_w that are compared with the UM results (section 5). Fuller details about the LEM-VOCALS simulation setup are provided in *Connolly et al.* [2013].

3.1.4. LEM-CONSTRAIN

The CONSTRAIN campaign took place during January 2010. The case analyzed features a strong northerly flow extending from latitudes higher than 70°N to the southern tip of the British Isles, with cold Arctic air moving south over the relatively warm Atlantic ocean. As the air travels over the water, moist convective processes cause it to gain heat and moisture, which can lead to organized convection [*Field et al.*, 2013; *McBeath et al.*, 2013]. The LEM is used here to produce a quasi-Lagrangian LES (LEM-CONSTRAIN simulation), in which a 50 by 50 km domain with horizontal resolution of 125 m is advected south-south east from (66° N, 11°W) to (60°N, 8°W) over the warmer seas to simulate the stratocumulus to cumulus transition. Initial conditions for the case are based on high-resolution limited area model simulations performed with the UM described in *Field et al.* [2013]. The change in SST represents the advection of the domain over warmer water. Fuller documentation is available at http://appconv.metoffice.com/cold_air_outbreak/constrain_case/crm_setup.html (latest access March 2014). The case is run for 15 h and outputs analyzed are for hours 03 to 05 (stratocumulus regime) and hours 12 to 15 (cumulus regime). Similarly, the LEM-CONSTRAIN results have been reinterpolated on a 1 by 1 km resolution grid to be compared with the UM outputs.

3.2. Unified Model Simulations at Kilometer-Scale Resolution

The UM is used to perform two set of simulations: the first set is a 2 day forecast for the 12 and 13 November 2008 over VOCALS-REx region dominated by a stratocumulus deck (UM-VOCALS simulations). In the second set, the UM produces a 34 h period forecast of a cold air outbreak in the north Atlantic for the 30 and 31 January 2010 (UM-CONSTRAIN simulations) where a transition from a stratocumulus to a cumulus regime is captured. The simulations are initialized from global model forecasts and successive model nesting at increasing resolution ultimately produces forecasts at a 1 km grid resolution (see appendix A for details). These 1 km model results will be used to apply our method and estimate the total vertical velocity variability. In addition, we perform a second cascade of nested high-resolution simulations for VOCALS-REx and CONSTRAIN, UM-HIRES-VOCALS, and UM-HIRES-CONSTRAIN, respectively, with model grid spacing varying between 500 m and 100 m (also see details in appendix A). These outputs will be used to evaluate if we can obtain consistent estimates of vertical velocity variability at different model resolutions with our methodology.

The UM-VOCALS simulation period is based on *Boutle and Abel* [2012]. Observations show a strong diurnal cycle in LWP, precipitation and boundary layer structure that is typical of this region of the southeast Pacific.

The 1 km model is 750 km (east-west) by 750 km (north-south) centered on 76°W, 20°S. The UM is initialized from a Met Office global analysis at 00:00 UTC on 12 November 2008. To ensure that the large-scale state of the atmosphere and ocean surface remains as close as possible to the truth throughout the study period, the global model is reinitialized from a global analysis at 00:00 UTC on 13 November 2008. The analyses are made with the instantaneous hourly outputs between 12-18 UTC during 12 November 2008 and 13 November 2008.

UM-CONSTRAIN 1 km domain is 750 km (east-west) by 1500 km (north-south) and centered approximately on 8°W, 62°N. The data presented here are from a run initialized from archived global analyses at 1200 UTC on 30 January 2010. The 1 km nested model runs from 1500 UTC on 30 January through to the end of 31 January 2010. The analyses are made with the instantaneous hourly outputs during 31 January 2010.

The UM cloud microphysics is a single-moment three-phase representation. For the liquid phase there are prognostic variables for cloud water and rain mixing ratio. For ice there is a prognostic variable for snow mass mixing ratio that represents all ice in the grid box. The basic formulation is described by *Wilson and Ballard* [1999] and fuller documentation by *Wilkinson* [2011]. A cloud scheme deals with subgrid humidity variations and cloud fraction [*Smith*, 1990]. For the UM-VOCALS simulation, the 1 km model runs with the autoconversion/accretion parametrization of *Khairoutdinov and Kogan* [2000] instead of the UM default *Tripoli and Cotton* [1980] and the rain drop size distribution derived in *Abel and Boutle* [2012] is used rather than the UM default *Marshall and Palmer* [1948] parametrization. UM-VOCALS and UM-CONSTRAIN simulation setups mirror the "best" configurations discussed in *Boutle and Abel* [2012] and *Field et al.* [2013], respectively, where fuller details are provided.

4. Construction of the Method to Account for Subgrid-Scale Updraft Velocity in Kilometer-Scale Models

4.1. Subgrid/Resolved Partitioning of Updraft Velocity Variability at Kilometer Scale

We seek to parameterize the missing subgrid vertical velocity variability in the large-scale model as a function of the resolved variability. To achieve that goal, we need to estimate the contribution of the resolved variability to the expected total variability at a given resolution. For that purpose, we will derive a partition function that separates the subgrid and resolved component using the LEM simulations and the aircraft observations. The following is presented in the context of the LES model (3-D domain) but the method remains similar for the aircraft data (1-D legs). Following *Dorrestijn et al.* [2013], we define three different length scales which are represented on Figure 1. The first length scale, L, represents the size of the horizontal domain in the LEM simulations. The second length scale, l, is the horizontal grid size of the LEM. Finally, the intermediate length scale Δ_x, lies in between L and l and can be seen as a length scale typical of a kilometer-scale model grid box where we would like to quantify the ratio of resolved/subgrid variability of vertical velocity. At each vertical level, the domain of size $L \times L$ contains $K = (L/\Delta_x)^2$ coarse subdomains of size $\Delta_x \times \Delta_x$. Each k^{th} coarse subdomain contains $J = (\Delta_x/l)^2$ grid point values $w_{j,k}$ of size $l \times l$ determined by the spatial resolution of the LEM. We define the following averages over the k^{th} subdomain and over the entire domain:

$$\overline{w}^{\Delta_x,k} = \frac{1}{J}\sum_j w_{j,k} \tag{1}$$

$$\overline{w}^{L} = \frac{1}{JK}\sum_{j,k} w_{j,k} = \frac{1}{K}\sum_k \overline{w}^{\Delta_x,k} \tag{2}$$

As showed in *Dorrestijn et al.* [2013], the total variability in updraft velocity can be expressed over the whole domain as

$$\overline{w'w'}^{L}_{\mathrm{tot}} = \frac{1}{K}\sum_k \overline{w'w'}^{\Delta_x,k} + \frac{1}{K}\sum_k \left(\overline{w}^{\Delta_x,k} - \overline{w}^{L}\right)^2 \tag{3}$$

where the superscript prime denotes the grid box deviation from the horizontal slab average, i.e., $w_{j,k} = w'_{j,k} + \overline{w}^{L}$. The first term on the right-hand side of equation (3) represents the subgrid contribution to the

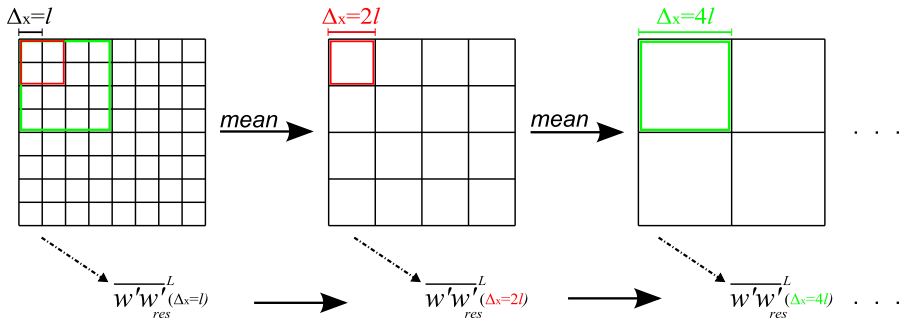

Figure 2. Coarse-graining principle applied to the high-resolution data sets (adapted from *Honnert et al.* [2011]). The first grid represents the native grid of the LES model at resolution $\Delta_x = l$. The coarse-graining procedure starts with averaging over all fine grid boxes of resolution l within coarse grid boxes each containing four fine grid boxes, leading to a coarse grid field at resolution $\Delta_x = 2/$(second grid), then within coarse grid boxes each containing 16 fine grid boxes, leading to a coarse grid field at resolution $\Delta_x = 4/$(third grid), and so on. The coarse fields are then used to calculate the resolved variability of updraft velocity at a given resolution (see text).

total variability that is not resolved at the scale Δ_x, hereafter denoted $\overline{w'w'}^{L}_{sgs}(\Delta_x)$, whereas the second term is the contribution of the fluxes that are resolved at scale Δ_x, hereafter denoted $\overline{w'w'}^{L}_{\mathrm{res}}(\Delta_x)$.

We define A as the ratio of the subgrid term over the resolved term

$$A(\Delta_x) = \overline{w'w'}^{L}_{\mathrm{sgs}}(\Delta_x) \Big/ \overline{w'w'}^{L}_{\mathrm{res}}(\Delta_x) \tag{4}$$

$$\overline{w'w'}^{L}_{\mathrm{tot}} = (1 + A(\Delta_x)) \times \overline{w'w'}^{L}_{\mathrm{res}}(\Delta_x) \tag{5}$$

To determine A at a certain grid size, we need to know the subgrid contribution to the vertical velocity variance which can be deduced by knowing the resolved part and the total variability. We first determine a reference total variability from the LEM results at grid resolution l

$$\overline{w'w'}^{L}_{\mathrm{tot}} = \overline{w'w'}^{L}_{\mathrm{res}}(l) + \overline{w'w'}^{L}_{\mathrm{sgs}}(l) \tag{6}$$

The resolved term is calculated with

$$\overline{w'w'}^{L}_{\mathrm{res}}(l) = \frac{1}{JK} \sum_{j,k} \left(w_{j,k} - \overline{w}^{L} \right)^2 \tag{7}$$

and we derive the subgrid part in the reference simulations from the subgrid TKE diagnostic of the LEM (representing, respectively, $\simeq 10\%$ and $\simeq 16\%$ of the total variability in the ASTEX and RICO simulations and we assumed no subgrid term in the OBS-VOCALS data set).

The total variability does not depend on the resolution; hence,

$$\overline{w'w'}^{L}_{\mathrm{res}}(\Delta_x) + \overline{w'w'}^{L}_{\mathrm{sgs}}(\Delta_x) = \overline{w'w'}^{L}_{\mathrm{res}}(l) + \overline{w'w'}^{L}_{\mathrm{sgs}}(l) \tag{8}$$

and subgrid part at grid size Δ_x can be expressed as

$$\overline{w'w'}^{L}_{\mathrm{sgs}}(\Delta_x) = \overline{w'w'}^{L}_{\mathrm{res}}(l) + \overline{w'w'}^{L}_{\mathrm{sgs}}(l) - \overline{w'w'}^{L}_{\mathrm{res}}(\Delta_x) \tag{9}$$

To calculate $\overline{w'w'}^{L}_{\mathrm{res}}(\Delta_x)$ we apply a coarse-graining procedure to the LEM results [*Shutts and Palmer*, 2007; *Honnert et al.*, 2011]. The initial fields of $w_{j,k}$ at resolution l are successively averaged horizontally at coarser scales up to the resolution L as illustrated in Figure 2. The values of $\overline{w'w'}^{L}_{\mathrm{res}}(\Delta_x)$ are obtain using the

Table 1. Cloud Base Vertical Velocity Length Scales (Z_{ml}) Used to Normalize the Horizontal Mesh Size

BL Type	Z_{ml}	Corresponding Data Set
M-STBL	$1.3\times Z_i$	LEM-ASTEX: hour 04 to 08
D-STBL	$0.5\times Z_i$	LEM-ASTEX: hour 12 to 30
C-STBL[a]	$0.5\times Z_i$	LEM-ASTEX: hour 30 to 36
C-STBL[b]	$h + h_c = Z_i$	LEM-ASTEX: hour 30 to 36
CBL	$h + h_c$	LEM-RICO: hour 24 to 36
D-STBL/M-STBL	$c_{\mathrm{ml}} \times Z_i$	OBS-VOCALS[c]

[a]At the stratocumulus layer base.
[b]At the cumulus layer base.
[c]For the VOCALS observations, we do not discriminate data into well-mixed or decoupled STBL. Instead, $c_{\mathrm{ml}} = Z_{\mathrm{ml}}/Z_i$ is computed separately for each leg using equations (14) and (15). Estimates are between 0.43 and 1.67 with a median of 0.76.

coarse-grained fields and calculated as in equation (7). Once the resolved part is known at the desired grid spacing, the subgrid part can be deduced from the total variance.

Finally, by dividing equation (9) by $\overline{w'w'}^{L}_{\mathrm{res}}(\Delta_x)$, we regain an expression for A:

$$A(\Delta_x) = \frac{\overline{w'w'}^{L}_{\mathrm{tot}}(l)}{\overline{w'w'}^{L}_{\mathrm{res}}(\Delta_x)} - 1 = \frac{1}{\sigma^*} - 1 \tag{10}$$

where we define σ^* as the partition function calculated from the coarse-graining analysis

$$\sigma^*(\Delta_x) = \frac{\overline{w'w'}^{L}_{\mathrm{res}}(\Delta_x)}{\overline{w'w'}^{L}_{\mathrm{tot}}(l)} \tag{11}$$

The equation (5) simply becomes

$$\overline{w'w'}^{L}_{\mathrm{tot}} = \frac{1}{\sigma^*(\Delta_x)} \times \overline{w'w'}^{L}_{\mathrm{res}}(\Delta_x) \tag{12}$$

The partition function provides an approximation of the ratio of resolved over total vertical velocity variability at a given grid resolution Δ_x. In section 4.4, we will discuss how to use the information from σ^* to correct the resolved vertical velocity variability in the UM from its missing subgrid part. But prior to that, we need to introduce a new variable, the dimensionless mesh size, to scale the cloudy boundary layer and assess a general form for partition function. This dimensionless mesh size is described in the following section.

4.2. Boundary Layer Scaling

The physical processes involved in the boundary layers considered in our LEM simulations and observations will produce different dynamics. Therefore, the scale of the turbulent mixing and transport of moisture and momentum will vary as well. As a result, we should not expect that the partition functions of the resolved/total vertical velocity variability will be identical for the different cases. Thus, we introduce a scaling for these boundary layers. *Honnert et al.* [2011] showed that a dimensionless mesh size, $\Delta_x/(h + h_c)$, is necessary to establish the partition function in the nonprecipitating convective boundary layer, where Δ_x is the horizontal mesh size, h is the dry boundary layer height, and h_c is the height of the cloud layer above the dry convective boundary layer if present. Using *Honnert et al.* [2011] as a basis, we define the appropriate length scale as Z_{ml}, the vertical velocity length scale in the cloud mixed layer, for the different regimes identified in the LES and aircraft observations data set. The definitions of Z_{ml} considered to normalize the grid mesh size in the different data sets are summarized in Table 1.

In the CBL, we follow *Honnert et al.* [2011]:

$$Z^{\mathrm{CBL}}_{\mathrm{ml}} = h + h_c \tag{13}$$

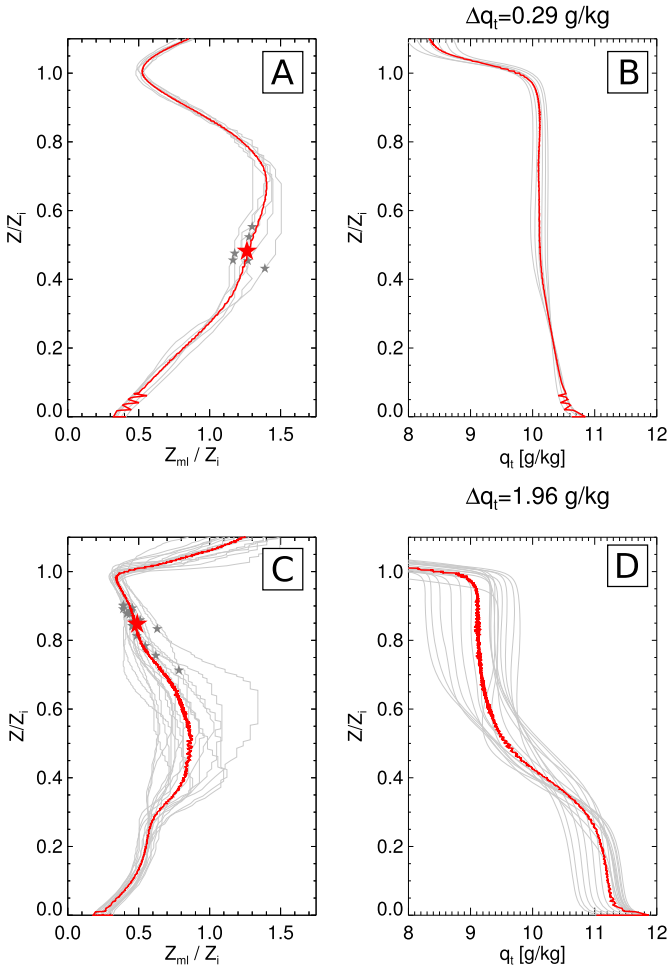

Figure 3. (a, c) Vertical velocity length scale normalized by boundary layer depth and (b, d) total water mixing ratio as a function of dimensionless height for the M-STBL regime (Figures 3a and 3b) and the D-STBL regime in LEM-ASTEX simulation (Figures 3c and 3d). The red curves represent the mean profiles for the respective regimes, whereas stars mark the mean stratocumulus cloud base. Δq_t is the difference in total water mixing ratio between the bottom 25% and the top 75% of the boundary layer.

where h is the depth of the surface mixed layer which marks the height of the lifting condensation level. The parameter h_c is the mean cloud depth above the subcloud surface mixed layer. The same formulation is assumed at the base of the cumulus layer in the C-STBL, but $h + h_c$ will mark the level of the inversion, Z_i.

In the M-STBL, we follow *de Roode et al.* [2004]:

$$Z_{\mathrm{ml}}^{\mathrm{M\text{-}STBL}} = \frac{1}{k_c} \tag{14}$$

where k_c is the spatial frequency above which two thirds of the variance remains

$$\frac{2}{3} < w'w' >_L = \int_{k_c}^{k_{NY}} S_w(k)dk \tag{15}$$

k_{NY} is the Nyquist frequency and $S_w(k)$ the power spectrum of w (see *de Roode et al.* [2004], for more details and justification about the factor 2/3). Figure 3a shows the vertical velocity length scale Z_{ml} normalized by the M-STBL inversion height Z_i. The latter was calculated in the LEM simulations as the altitude where the mean profile of the vertical gradient of the buoyancy flux is minimum. Within the first half of the cloud layer, the ratio of Z_{ml} over Z_i is maximum and approximately equal to 1.3. The physical meaning is that the velocity structures at these altitudes are roughly 30% larger than the depth of the boundary layer in the well-mixed STBL for this case, i.e., the largest eddies which carry most of the energy are stretched in the horizontal and

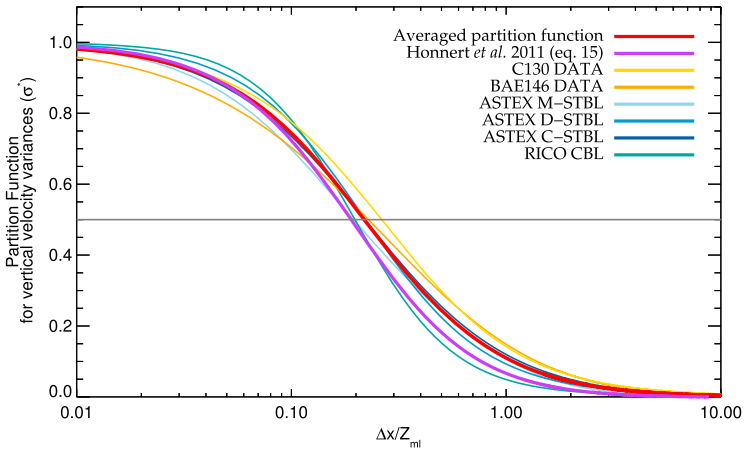

Figure 4. Resolved vertical velocity variance partition (σ^*) versus the dimensionless mesh size.

have a characteristic length scale bigger than the boundary layer depth. Hence, we will use $Z_{\mathrm{ml}}^{\mathrm{M\text{-}STBL}} = 1.3 \times Z_i$ to normalize the mesh size in the M-STBL. It is likely that the ad hoc 1.3 value may be case dependent and could vary for other M-STBL (e.g., with the intensity of the LW radiative cooling at the top). *de Roode et al.* [2004] suggest that Z_{ml} is a function of r, the ratio of the entrainment to surface fluxes of w (i.e., $r = < w'w' >_{z=\mathrm{top}} / < w'w' >_{z=\mathrm{srf}}$). This would require further investigation which is beyond the scope of that study.

In the D-STBL, the mesh size is normalized by $Z_{\mathrm{ml}}^{\mathrm{D\text{-}STBL}} = 0.5 \times Z_i$ and the factor 0.5 is derived analogously as in the M-STBL (see Figure 3c). This can be seen as a representation of the length scale of mixing in the decoupled stratocumulus layer. Profiles of total water content (Figure 3d) agree as it can be seen that the decoupled stratocumulus layer depth is encompassed between 0.4 and 0.6 times Z_i. The same formulation is assumed at the base of the stratocumulus layer in the C-STBL.

4.3. Determining the Partition Function

Following the methodology described in sections 4.1 and 4.2, we can now construct the partition function of vertical velocity variances. We have computed the fields of w at coarser resolution for data at or slightly above cloud base level as, our final application will be aerosol activation. The curves representing the partition functions for the different BL regimes are shown in Figure 4. These curves are obtained using a least squares fitting routine on the variances calculated from the coarse-grained updraft velocity fields for the respective data set. For comparison purposes, we have also overlaid the partition function of TKE from *Honnert et al.* [2011] results. The good agreement between these functions suggests that we can infer a general (averaged) partition function. Such a partition function of the resolved vertical velocity can be represented with the following functional form:

$$\sigma^*\left(\frac{\Delta_x}{Z_{\mathrm{ml}}}\right) = 1 - \frac{\left(\frac{\Delta_x}{Z_{\mathrm{ml}}}\right)^{E1} + a \times \left(\frac{\Delta_x}{Z_{\mathrm{ml}}}\right)^{E2}}{\left(\frac{\Delta_x}{Z_{\mathrm{ml}}}\right)^{E1} + b \times \left(\frac{\Delta_x}{Z_{\mathrm{ml}}}\right)^{E2} + c} \tag{16}$$

with a = 7.95, b = 8.00, c = 1.05, E1 = 2.59, and E2 = 1.34 for the averaged partition function (i.e., red curve in Figure 4). The following section will discuss how to use the information that equation (16) provides to assess the SGS variability in the UM.

4.4. Assessing the Resolved Updraft Velocity Variability in the Kilometer-Scale Model

The final step in our framework consists of assessing the resolved variability of w at the resolution of the kilometer-scale model (equations (3) and (12)). For each grid point in the UM, we construct the resolved part of w variances using the information from the adjacent grid boxes. It is defined as follows: first, we construct a horizontal domain centered on the given grid point. The domain size is $L \times L$ as in Figure 1 and is chosen to be $\mathcal{O}(10 - 20\ \mathrm{km}^2)$ to be consistent with the domains in the LES considered to construct the partition function. For instance, for a UM simulation at resolution $\Delta_x = 1$ km, the surrounding domain is made of $N = 19 \times 19$ grid boxes (i.e., the 9 nearest neighbor grid boxes in the x and y directions surrounding the

central point). Similarly, at a model resolution $\Delta_x = 333$ m, the surrounding domain is made of $N = 59 \times 59$ grid boxes (i.e., the 29 nearest neighbor grid boxes). Then, we calculate the resolved variances at resolution Δ_x for the central grid point over this domain.

Finally, we need to introduce a term in equation (12) to account for potential underestimation of the resolved term of vertical velocity variability in the large-scale model, i.e., term $\overline{w'w'}^L_{\text{res}}(\Delta_x)$ in equation (12). If we assumed that the resolved term computed in the large-scale model is representative of the grid resolution Δ_x of the model, then no correction is necessary. However, models have an effective resolution that is coarser than the model grid resolution by usually a factor of 4 to 10 depending on the numerical formulation of the model (e.g., semi-Lagrangian/semi-implicit versus explicit Eulerian advection schemes) [*Skamarock*, 2004; *Tonttila et al.*, 2011; *Ricard et al.*, 2012]. For the length scales smaller than the effective resolution, the diffusion of the resolved dynamical scalars in the high frequencies of the power spectrum tends to damp the energy; therefore, it is likely that $\overline{w'w'}^L_{\text{res}}(\Delta_x)$ will be underestimated. To account for that effect, we simply reformulate the total vertical velocity variability as

$$\overline{w'w'}^L_{\text{tot}} = f \times \frac{1}{\sigma^*} \times \overline{w'w'}^L_{\text{res}}(\Delta_x) \tag{17}$$

where, f is an ad hoc factor to account for these effects. The appropriate value of f would depend on the numerical formulation of the model and its configuration. By default, we let $f = 1$. In the results (section 5) we will show that $f = 4$ provides a reasonable correction for our current configuration of the Unified Model. Characterizing the UM effective resolution and its implications would require a significant number of extra simulations and analysis which is beyond the scope of this paper.

We can now calculate the total variability from equation (17) knowing the resolved variability at the resolution of the kilometer-scale model and the expected value of σ^* at this same resolution by using the partition function established above.

4.5. Implementation in the Unified Model

To implement the method in the Unified Model, we need to calculate on the fly the values of the partition function. The model resolution (Δx) is obviously known; hence, it remains to assign the proper horizontal scaling (Z_{ml}) to compute the dimensionless mesh grid (i.e., $\Delta x/Z_{\text{ml}}$). This depends on the boundary layer regimes. We will use the diagnostics of the *Lock et al.* [2000] boundary layer scheme present in the UM to calculate Z_{ml}. This scheme handles the mixing in the vertical using a nonlocal 1-D boundary layer scheme [*Lock et al.*, 2000; *Lock*, 2011]. It generates a diagnosis of boundary layer "type" based on the surface buoyancy flux and profiles of potential temperature, winds, and humidity. The type assigned determines the rules for the nonlocal mixing throughout the lower troposphere. Seven types of boundary layers (BL I to VII) are identified and named as follows:

BL I: Stable b. layer, possibly with nonturbulent cloud
BL II: Stratocumulus over a stable surface layer
BL III: Single-mixed layer, possibly cloud topped
BL IV: Decoupled stratocumulus not over cumulus
BL V: Decoupled stratocumulus over cumulus
BL VI: Cumulus-capped layer
BL VII: Shear-driven boundary layer

The boundary layer scheme diagnostics associated with each boundary layer type are used to define Z_{ml} in a fashion which should be consistent with the boundary layer definitions given in section 3.1 and Table 1; For BL type III (i.e., equivalent to the M-STBL), we diagnose the horizontal scaling Z_{ml} as being equal to 1.3 times the depth of the boundary layer which is defined from the surface diffusivity profile K_{surf}. For BL II and BL IV (i.e., equivalent to the D-STBL), Z_{ml} is diagnosed from the depth defined by the stratocumulus diffusivity profile K_{sc}. The same definition of Z_{ml} is applied at the stratocumulus layer base in BL V (i.e., equivalent to the C-STBL). For BL type VI (i.e., equivalent to the CBL), Z_{ml} is diagnosed from the highest altitude reached by an air parcel rising from the surface. The same definition of Z_{ml} is applied at the cumulus layer base in BL V (i.e., equivalent to the C-STBL). The BL types I and VII were not represented in the LEM simulations and observation data sets considered to construct the partition function. We will then assume a similar scaling as in BL IV for these two cases. However, occurrence for these two types remains low in the UM simulations that will be analyzed in the results section (not shown). Note that in the UM-HIRES-VOCALS and UM-HIRES-CONSTRAIN

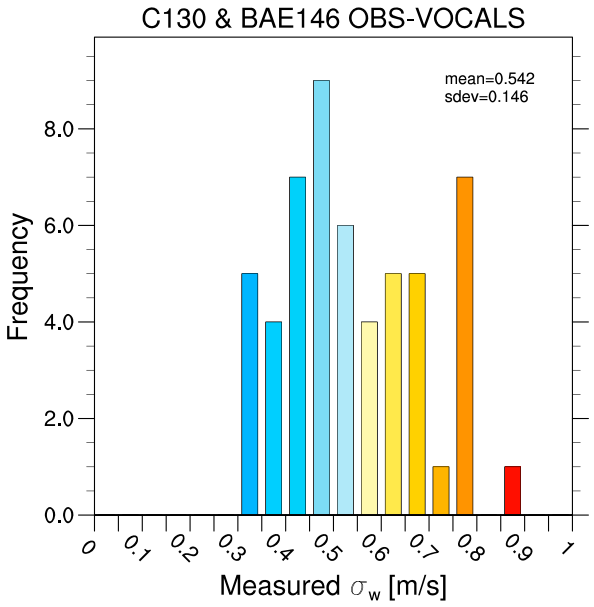

Figure 5. Histogram of the vertical velocity standard deviation from aircraft observations measured during VOCALS (see section 3.1.3).

simulations, the vertical mixing is handled by a 3-D scheme following the method of *Smagorinsky* [1963]. In the present configuration of the UM, the *Lock et al.* [2000] boundary layer scheme is switched off when the Smagorinsky-type scheme is activated. Therefore, we have a posteriori diagnosed the boundary layer depths and cloud heights based on the profiles of potential temperature and specific humidity simulated by the UM. Although the UM boundary layer scheme uses trigger functions which produce artificially sharp transitions between meteorological regimes hence discontinuities in Z_{ml}, we have observed that the diagnosed Z_{ml} exhibit relatively organized patterns as certain boundary layers types are more predominant than others as the model integration is carried on. Sensitivity experiment (not shown) using a constant and similar definition of Z_{ml} for all BL types suggests that our estimates of $\overline{w'w'}_{tot}$ are not significantly modified. Therefore, the activation behavior over the whole domain should not be affected significantly by discontinuities in Z_{ml}.

5. Results

5.1. VOCALS: 12–13 November 2008

5.1.1. LEM-VOCALS and OBS-VOCALS

Prior to discussing the UM 1 km model results, we introduce the LEM results and the aircraft observations used to evaluate and constrain our modeling framework. We first focus on the aircraft measurement statistics. During the 2 day period of the UM-VOCALS forecast, only two BAe-146 research flights (RF 419 and RF 420) and one C-130 research flight (RF 13) are available. Consequently, the number of near–cloud base legs that can be used to compare with the UM-VOCALS outputs is relatively small. In addition we do not expect that the few model grid points closest to the individual legs (of lengths of between 25 and 140 km, or 5 and 20 min in duration) can mirror these observations at the given model resolution. To give us some estimation of the vertical velocity variability in the observations, we have therefore used the 55 in-cloud legs described in section 3.1.3 which were sampled during the whole campaign period to compute leg-averaged statistics of the vertical velocity standard deviation (Figure 5). The mean standard deviation from this data set is 0.54 m s^{-1} which is in good agreement with the mean values (approximately 0.4 to 0.6 m s^{-1}) reported in *Bretherton et al.* [2010]. It is noted that none of the leg-averaged standard deviations in Figure 5 are below 0.3 m s^{-1} which might suggest relatively high estimates in our sample. This could be in part explained by the relatively low number of leg averages considered (55) that may not be sufficient to statistically represent the full spectrum of vertical velocity standard deviations within stratocumulus clouds. Furthermore, among selection criteria for the near cloud base legs, we have retained legs with relatively constant and high LWC. The thicker the cloud layer is, the stronger the LW radiative cooling at cloud top is. The cloud layer hence generates more in-cloud turbulence, and this could have potentially shifted our statistics of σ_w toward higher values.

In order to further constrain our results, we have also looked at outputs from the LEM-VOCALS simulation. Figure 6 (right) presents the vertical profile of the vertical velocity standard deviation from the LEM-VOCALS simulation. The profile exhibits a double-peak structure illustrating the start of the decoupling between the cloud layer and the surface mixed layer although the whole boundary layer remains relatively mixed for this time of the simulation (not shown). The cloud base is at approximately 972 m and the corresponding statistics of σ_w at this model level are also represented on Figure 6. The mean σ_w from LEM-VOCALS at cloud base is equal to 0.38 m s^{-1}.

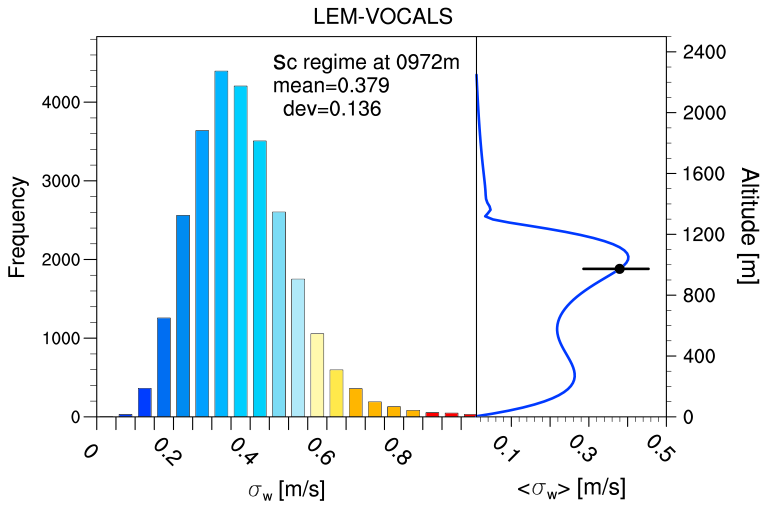

Figure 6. VOCALS (left) histogram of the cloud base vertical velocity standard deviation and (right) mean profiles of the vertical velocity standard deviation from the LEM runs. The black dots mark the averaged cloud base altitude in the simulation. Bars are representing the lower and upper quartiles of the cloud base vertical velocity standard deviation. Prior to constructing the histogram, the standard deviations have been reaggregated at 1 km resolution for consistent comparison with the UM results.

Compared to the value of 0.54 m s^{-1} derived from the aircraft observations, the mean estimate in LEM-VOCALS is lower. However, one can argue that the relatively coarse resolution of this idealized LES setup might result in an underestimation of the variability in updraft velocity, whereas, as previously discussed, the observations mean estimate might be biased toward higher values. In that sense it is reasonable to consider that the range given by these two independent techniques could be representative for stratocumulus clouds over the south east Pacific.

5.1.2. UM-VOCALS 1 km Model

Figures 7a and 7b illustrate the estimates, i.e., the resolved term in equations (3) and (17) and discussed in section 4.4, of vertical velocity standard deviation, σ_w (with $\sigma_w = \sqrt{\overline{w'w'}^L}$), from the UM-VOCALS 1 km simulations for the 12 November 2008 and 13 November 2008, respectively . The vertical velocity standard deviation estimates are shown at an altitude of 955 m which is a representative altitude for the mean cloud base as observed during the campaign period over the VOCALS region [see *Bretherton et al.*, 2010, Figure 12]. In these results, the "uncorrected" values of the vertical velocity standard deviation range approximately between 0.02 and 0.14 m s^{-1} over the 1 km model domain with the highest values occurring within the regions where the UM is able to simulate the organization of closed cellular convection [*Boutle and Abel*, 2012]. Once our framework is applied, the "corrected" estimates of σ_w using the default value $f = 1$ in equation (17) (Figures 7c and 7d) now range approximately between 0.05 and 0.6 m s^{-1} illustrating the dominant contribution from the subgrid component when the UM is operating at 1 km resolution. The new estimates are in better agreement with observation results. For example, using in-cloud legs data from the C-130 aircraft, *Bretherton et al.* [2010] evaluate mean standard deviations of about 0.4–0.6 m s^{-1} during the VOCALS observation period. In the tropical Atlantic, during ASTEX, *de Roode and Duynkerke* [1997] show values ranging from approximately 0.22 to 0.45 m s^{-1} at cloud base. *Peng et al.* [2005] report an averaged value of 0.23 m s^{-1} from the observations sampled in the northwest Atlantic during the North Atlantic Regional Experiment and the Radiation, Aerosol and Cloud Experiment while *Lu et al.* [2007] report relatively small estimates from 0.06 to 0.29 m s^{-1} from measurements in the northeast Pacific offshore of California during Marine Stratus/Stratocumulus Experiment (MASE). Slightly higher values at cloud base spanning from 0.27 to 0.55 m s^{-1} have also been observed during second Aerosol Characterization Experiment (ACE-2) in the northeast Atlantic [*Guibert et al.*, 2003].

However, because there is generally little consistency between different campaigns (length of flight legs, the selection criteria with which clouds were chosen, the instrumentation used to make measurements, the altitude of measurements, the dynamical state of the boundary layer during the time of sampling, etc.),

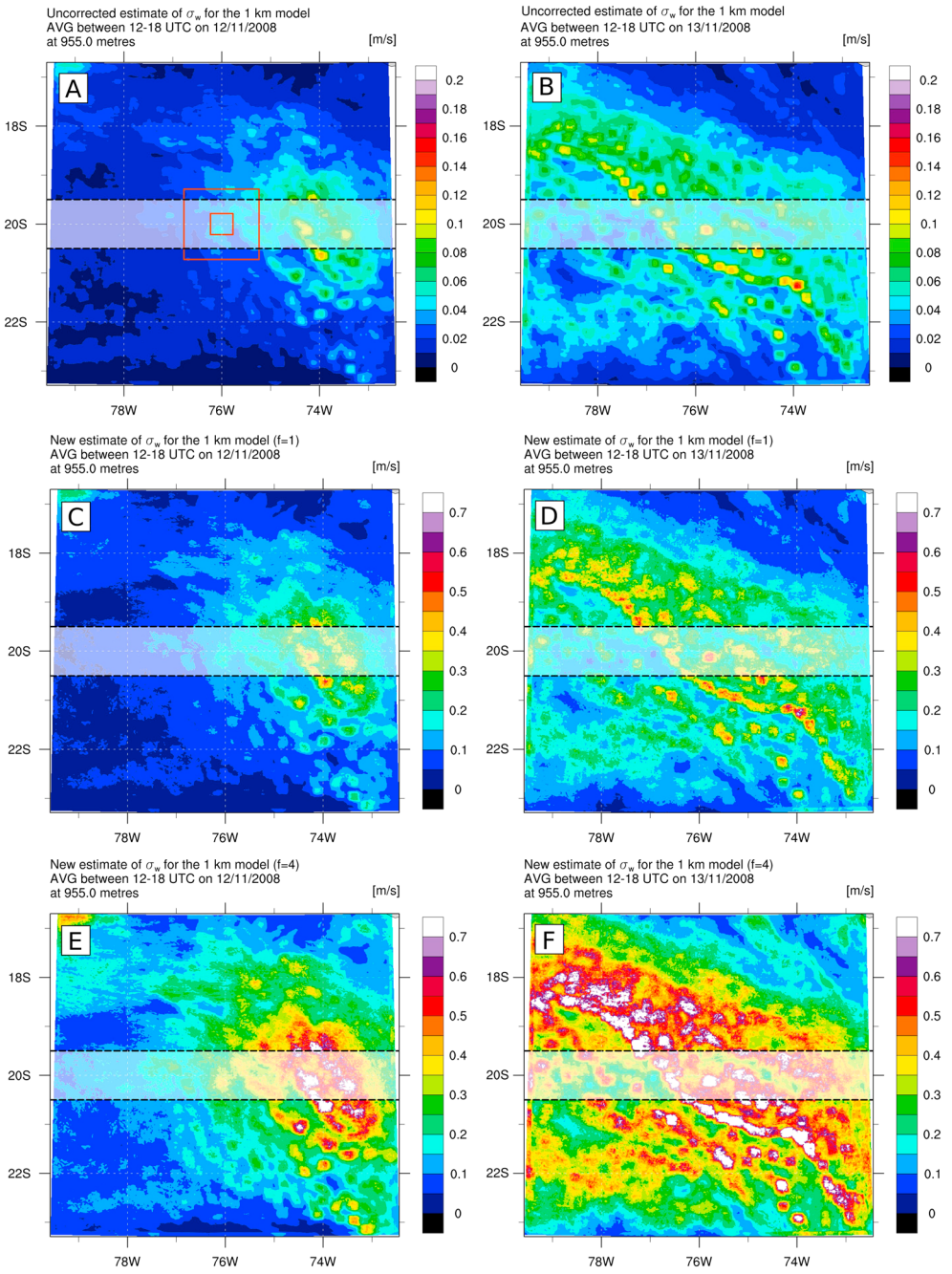

Figure 7. Estimates of vertical velocity standard deviation from the UM simulation at 1 km horizontal resolution over VOCALS region for (a, c, and e) the 12 November 2008 and (b, d, and f) the 13 November 2008. Figures 7a and 7b represent the raw (resolved) estimates of vertical velocity standard deviation. Figures 7c and 7d represent the corrected (resolved + subgrid) estimate of vertical velocity standard deviation ($f = 1$ in equation (17)). Figures 7e and 7f represent the corrected (resolved + subgrid) estimate of vertical velocity standard deviation increased by a factor 2, i.e., $f = 4$ in equation (17) (see text for justification). The orange squares in Figure 7a mark the limits of the UM nested high-resolution simulations at, respectively, 333 m and 100 m horizontal resolution (see text).

assessing a typical range of values of the vertical velocity standard deviation that characterizes stratocumulus clouds is challenging. Therefore, to evaluate the pertinence of our results, we will adopt a statistical approach for the comparison with the observational data and idealized LES runs. We focus the analysis on the subdomain represented by the grey shading on Figure 7 which is the area 1° in width along the 20°S transect where most of the VOCALS research flights were performed. We will assume that the statistics

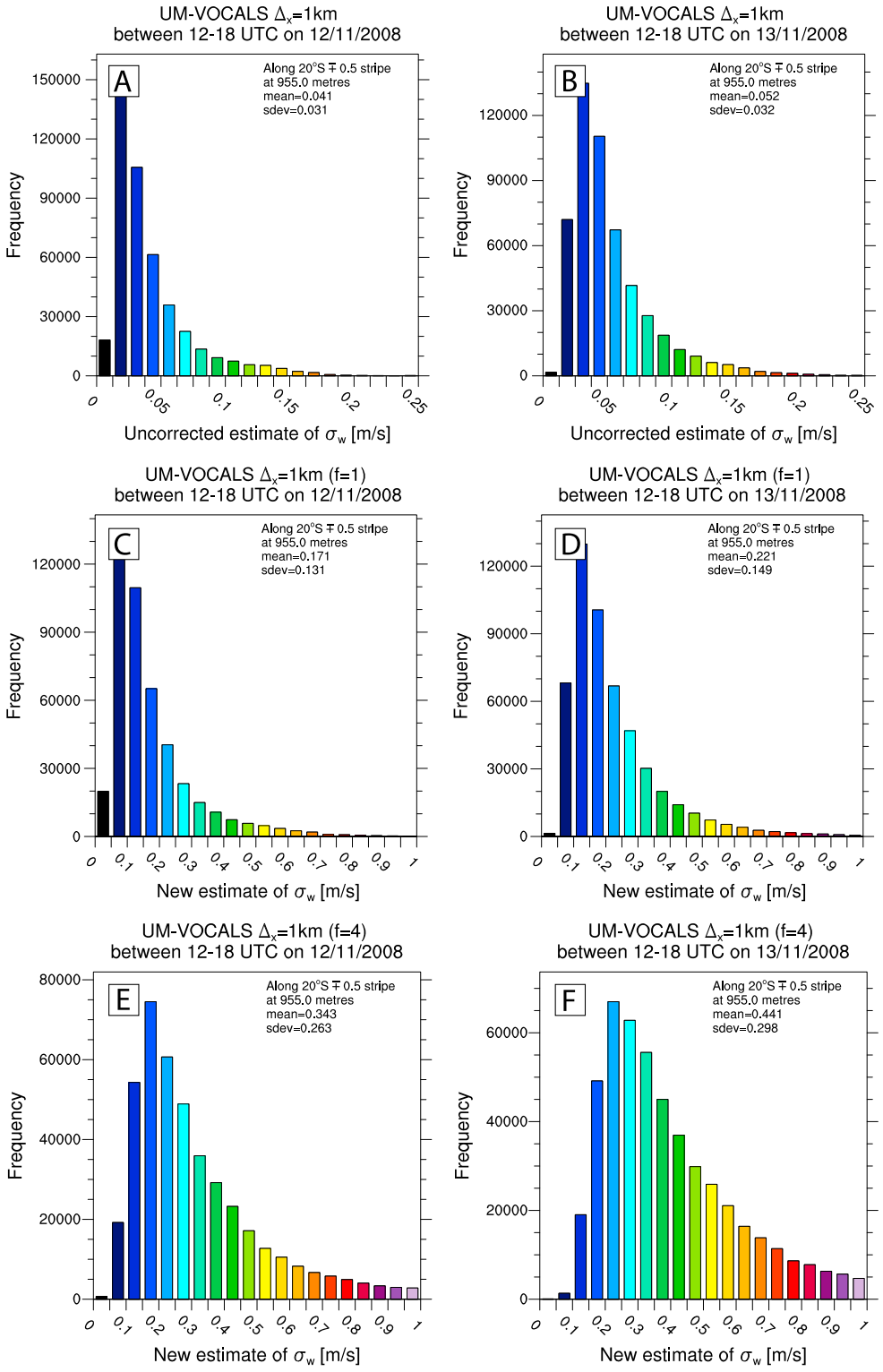

Figure 8. Statistics of vertical velocity standard deviation from the UM simulation at 1 km horizontal resolution over VOCALS region for (a, c, and e) the 12 November 2008 and (b, d, and f) the 13 November 2008. Figures 8a and 8b represent the raw (resolved) estimates of vertical velocity standard deviation. Figures 8c and 8d represent the corrected (resolved + subgrid) estimate of vertical velocity standard deviation ($f = 1$ in equation (17)). Figures 8e and 8f represent the corrected (resolved + subgrid) estimate of vertical velocity standard deviation increased by a factor 2, i.e., $f = 4$ in equation (17) (see text for justification). Note that the *y* axes are not the same for the different histograms.

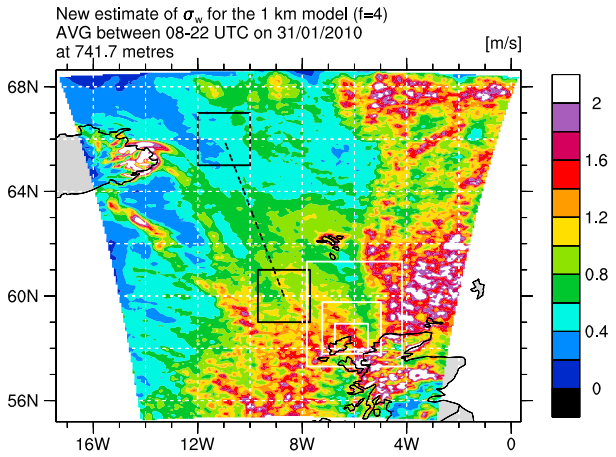

Figure 9. Estimates of corrected (resolved + subgrid) vertical velocity standard deviation from the UM-CONSTRAIN simulation at 1 km horizontal resolution during the 31 January 2010. The grey squares mark the limits of the UM nested high-resolution simulations at, respectively, 500 m, 200 m, and 100 m horizontal resolution (see text). The black square north (respectively, south) of the domain represents the area of the stratocumulus (respectively, cumulus) regime considered to compute the histogram in Figure 11.

computed over this subdomain for the 2 day UM-VOCALS forecast are representative of the VOCALS region and can be compared with the mean campaign statistics.

Figures 8a and 8b show the histograms of the uncorrected vertical velocity standard deviations for the 12 and 13 November 2008, respectively, at the altitude of 955 m over the 20°S transect subdomain, whereas Figures 8c and 8d show the histograms for the same periods and locations of the corrected values once the subgrid term is taken into account. When SGS variability is not considered, the mean standard deviations are 0.04 and 0.05 m s^{-1}, which is roughly an order of magnitude lower than usually reported in literature. On the other hand, the mean of the corrected estimates lie between 0.171 and 0.221 m s^{-1} (using the default value $f = 1$ in equation (17)). For this case study, the application of our framework corresponds to an approximate increase of a factor of 4.2 in vertical velocity standard deviation. In comparison, the UM-VOCALS means of σ_w are approximately a factor 2 lower than in the observations and in the LEM-VOCALS (section 5.1.1).

As introduced in section 4.4, we hypothesize that this underestimation may relate to the effect of model effective resolution on the resolved term of vertical velocity variability in the large-scale model. Using these results as a basis, we modify the default value $f = 1$ in equation (17) to $f = 4$. Figures 7e, 7f, 8e, and 8f show the estimates of σ_w for the 2 days of UM-VOCALS forecasts using equation (17) with $f = 4$. On 12 November 2008 and 13 November 2008, the mean estimates of σ_w over the 20°S transect are now, respectively, equal to 0.34 and 0.44 m s^{-1} which compares well with the observations estimate (0.54 m s^{-1}) and LEM-VOCALS estimate (0.38 m s^{-1}). This correction to the resolved term in the application of our framework, corresponds to an approximate factor 8.1 increase in vertical velocity standard deviation. In the remainder of this study, we will conserve this formulation of $\overline{w'w'}^{l}_{\mathrm{tot}}$ in equation (17), i.e., $f = 4$, to test our framework on the CONSTRAIN cold air outbreak case.

5.2. CONSTRAIN: 30–31 January 2010

Here we present the results for the UM-CONSTRAIN simulations. This case simulates a strong northerly flow, where a transition from a stratocumulus to a cumulus regime is observed as the cold Arctic air moves south over the relatively warm Atlantic ocean. We will focus the analysis on two regions over the 1 km UM-CONSTRAIN domain. The first region (northwest of the domain) is the region dominated by the stratocumulus regime; while the second region (south of the domain) is the region dominated by the convective regime. The statistics presented here will be computed over these regions which are represented by the grey shades within the black boxes on Figure 9.

Figure 9 shows the averaged σ_w for the 31 January 2010 over the 1 km UM-CONSTRAIN domain with the SGS variability taken into consideration. The averages range approximately between 0.2 and 1.5 m s^{-1} over most of the domain but can reach higher values up to 2 ms^{-1} or above. This is significantly higher than the estimates obtained in the UM-VOCALS simulations but should be expected given the strong

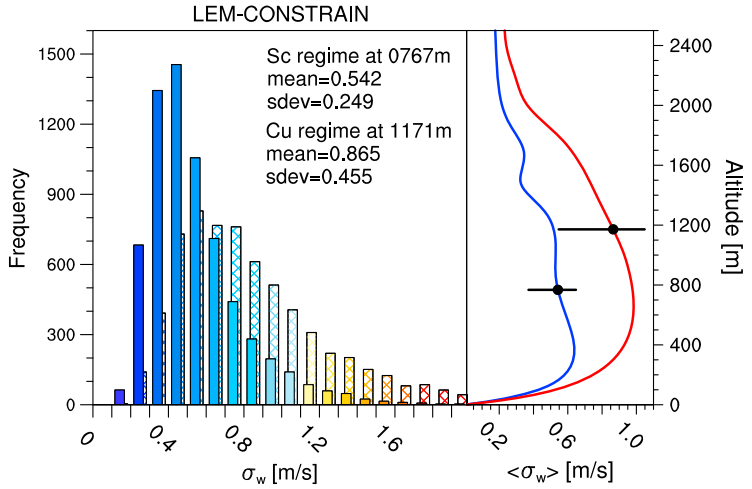

Figure 10. Similar to Figure 6 but for the LEM-CONSTRAIN simulation. The plain (respectively, dashed) bars in the histogram correspond to the stratocumulus (respectively, cumulus) regime in the CONSTRAIN simulation (see text).

contrast in temperature between the cold Arctic air and the warmer ocean which favors the triggering of vigorous convection. The LEM-CONSTRAIN simulations support this, as can be seen in Figure 10 which presents the vertical profiles of the vertical velocity standard deviation for the two regimes. The cloud base is approximately 767 m for the stratocumulus regime (respectively, 1195 m for the convective regime) and the corresponding histogram of σ_w at this model level are represented on Figure 10. The mean σ_w from LEM-CONSTRAIN at cloud base is equal to 0.54 m s^{-1} for the stratocumulus regime and 0.87 m s^{-1} for the cumulus regime with a broadening of the histogram of σ_w as the convective regime begins to dominate. The equivalent UM-CONSTRAIN histogram for the 1 km model are shown in Figure 11. Over the stratocumulus area, the mean estimate of σ_w is 0.45 m s^{-1} whereas over the cumulus area, the mean estimate of σ_w is 0.86 m s^{-1}. These results compare well with the LEM-CONSTRAIN results. This seems to indicate that we can have some confidence in the methodology developed here and it also suggests that the proposed framework may be used for a wider range of applications than tropical marine boundary layer clouds. The application of our framework for this case study corresponds to an approximate increase of a factor 4.8 in vertical velocity standard deviation, which is less than in the UM-VOCALS simulations (i.e., approximately 8.1). The reason for this relies on the fact that the boundary layer reaches higher altitudes in the CONSTRAIN simulations due to the strong convection. Hence, the dimensionless mesh grid is lower as is the unresolved variability of w.

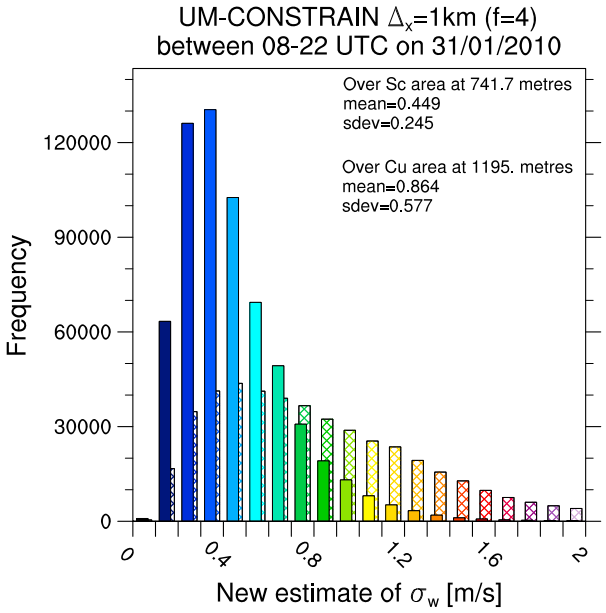

Figure 11. Statistics of vertical velocity standard deviation from the UM simulation at 1 km horizontal resolution over CONSTRAIN region for stratocumulus (plain bars) and cumulus (dashed bars) regimes.

5.3. Consistent Estimates of Vertical Velocity Variability at Different Model Resolutions: UM Nested Simulations Results

In the previous sections, we have compared the results from the UM simulations for the 1 km models with observations and LEM simulations to ensure that the framework we have developed is able to generate vertical velocity variability with the correct order of magnitude. We also evaluate if we can still obtain consistent estimates of vertical velocity variability at different model

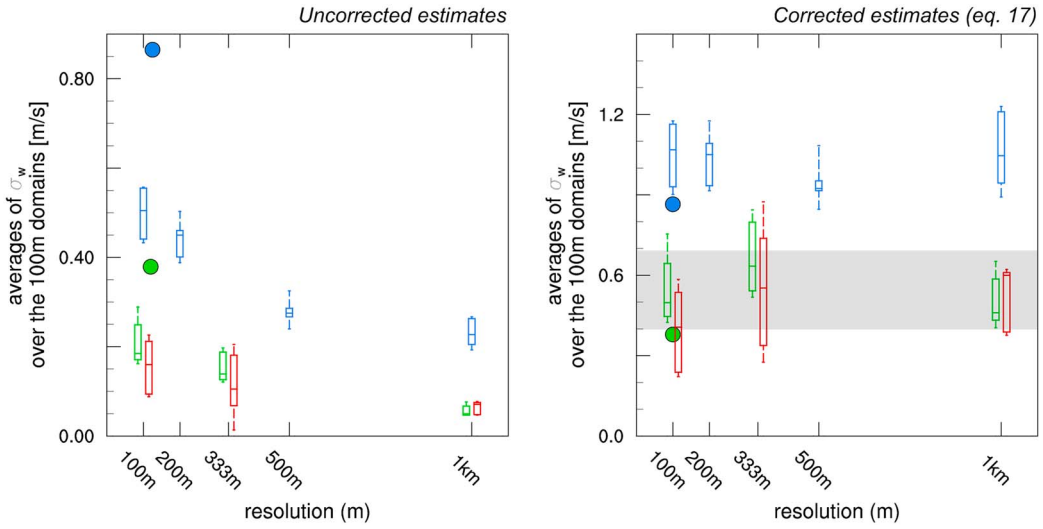

Figure 12. Box-and-whisker plots showing minimum, 25th percentile, median, 75th percentile, and maximum values of averages of vertical velocity standard deviation from the UM simulation over the 100 m model domains versus model horizontal resolution. (left) The resolved and (right) total (using f=4 in equation (17)) standard deviations of vertical velocity for UM simulations of (blue) CONSTRAIN on the 31 January 2010 and VOCALS on the 12 November 2008 (green) and 13 November 2008 (red). The filled dots represent the domain average σ_w from LEM simulations while the grey shading represent the VOCALS aircraft observation mean $\pm$ one standard deviation.

resolutions. The results discussed here are comparisons of the averaged σ_w from UM-HIRES-VOCALS (Δ_x = 333 m and Δ_x = 100 m) and UM-HIRES-CONSTRAIN (Δ_x = 500 m, Δ_x = 200 m, and Δ_x = 100 m, domains are shown in Figures 7 and 9) with the 1 km model results (UM-VOCALS and UM-CONSTRAIN). The averaged σ_w have been computed for all models over the area covered by the domain of the respective 100 m nested models.

Figure 12 (left) shows the vertical velocity standard deviations from the different models versus model resolutions when the SGS variability is not taken into account. This shows that without correction, the variability of updraft velocity systematically decreases with model resolution as anticipated, i.e., the coarser the resolution, the lower the variability that is resolved. Applying our framework to take into account the SGS variability leads to estimates of vertical velocity variability that are now consistent independently of model resolution for the different model simulations (Figure 12, right). For instance, the medians of σ_w for the CONSTRAIN case study are 1.07, 1.05, 0.92, and 1.05 m s^{-1} for model resolutions of 100 m, 200 m, 500 m, and 1 km, respectively.

In addition, the domain averages of σ_w at mean cloud base from the 125 m horizontal resolution LEM simulations (Figures 6 and 10) are also shown in Figure 12. Although the LEM simulation domains do not completely encompass the same area and period as the UM 100 m models, it is interesting to compare the two model results. The LEM estimates are approximately a factor of 2 larger than the uncorrected results from the UM models operating at very nearly the same horizontal resolution. This result reflects the differences in the UM and LEM numerical formulations. The scale of the finest fully resolved modes is primarily dependent on implicit and explicit diffusion. The LEM, a large eddy simulation model is less dissipative than a model using semi-Lagrangian/semi-implicit treatment of the advection such as the UM. Hence, it is not surprising to observe that, for the same resolution, the resolved estimates of vertical velocity variability are larger in the LEM than in the UM [e.g., *Ricard et al.*, 2012].

6. Implication for CCN Activation

We have shown that the contribution of the SGS variability of vertical velocity is significant, if not dominant, even for a model operating at a grid resolution of 1 km or less. In this section we seek to investigate the sensitivity of activation parametrization results depending on updraft velocities assumptions (e.g., with or without SGS variability) within the model grid boxes. We use the *Shipway and Abel* [2010] activation

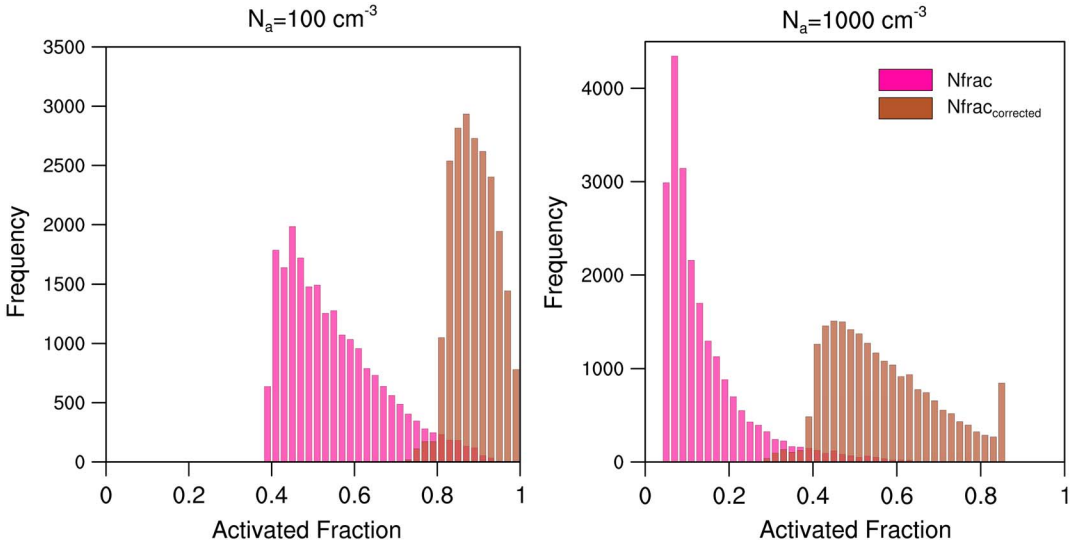

Figure 13. Histogram of aerosol activated fraction from off-line calculations over the VOCALS 20°S transect subregion (see section 5.1.2) for initial aerosol concentrations of (left) 100 cm^{-3} and (right) 1000 cm^{-3}. The brown (pink) bars represent the activated fraction calculated when (not) considering the SGS updraft velocity correction.

scheme to perform off-line calculations of CCN-activated fraction using the estimates of σ_w from the UM-VOCALS 1 km model simulation as inputs. Calculations are initialized at temperature of 279 K and pressure of 1000 hPa. We assume an idealized marine aerosol environment, with an aerosol distribution composed of ammonium sulfate with a single accumulation mode represented by a lognormal distribution given by $\sigma = 2$, a geometric radius $r_d = 60$ nm, and varying number concentrations.

The updraft velocity inputs considered here are the instantaneous values from the 20°S transect subregion in the UM-VOCALS 1 km model (grey area in Figure 7), for an altitude of 955 m (near cloud base), at 14:00 UTC on the 13 November 2008. The activation scheme has been run for each model grid box (i, j) with and without considering the SGS variability of updrafts. In the first case, the model grid box resolved vertical velocities w, are used to calculate the maximum supersaturation and activated number within the activation parametrization. In the second case, corrected vertical velocities (w_{corr}) which consider the SGS contribution are used. These are derived from rescaling the w field such as the corrected variances match the one derived from our method

$$w_{\mathrm{corr}}(i,j|\Delta_x) = a \times w(i,j|\Delta_x) \quad \text{and} \quad \overline{w'w'}^{L}_{\mathrm{corr}}(i,j|\Delta_x) = \overline{w'w'}^{L}_{\mathrm{tot}}(i,j|\Delta_x) \tag{18}$$

Dropping the dependency on Δ_x, the definition of the variances gives

$$\overline{w'w'}^{L}_{\mathrm{tot}}(i,j) = \frac{1}{N^2}\sum_{i,j-N/2}^{i,j+N/2}\left(w_{\mathrm{corr}}(i',j') - \overline{w}^{L}\right)^2 = \frac{1}{N^2}\sum_{i,j-N/2}^{i,j+N/2}\left(a \times w(i',j') - \overline{w}^{L}\right)^2 \tag{19}$$

with $N = L/\Delta_x$ and noting that the mean velocities over $L \times L$ are ~0 m s^{-1}

$$\overline{w'w'}^{L}_{\mathrm{tot}}(i,j) \simeq \left(\frac{a}{N}\right)^2 \sum_{i,j-N/2}^{i,j+N/2}\left(w(i',j')\right)^2 \simeq a^2 \times \overline{w'w'}^{L}_{\mathrm{res}}(i,j) \tag{20}$$

Hence,

$$w_{\mathrm{corr}}(i,j) = w(i,j) \times \sqrt{\frac{\overline{w'w'}^{L}_{\mathrm{tot}}(i,j)}{\overline{w'w'}^{L}_{\mathrm{res}}(i,j)}} \tag{21}$$

The activation scheme is only run for grid boxes with positive velocities.

Figure 13 shows histograms of aerosol activated fraction calculated over the VOCALS 20°S transect subdomain. For a clean aerosol environment ($N_a = 100$ cm^{-3}), the median activated fraction is 0.52 when model

uncorrected velocities are used. Once the SGS variability is considered, most of the aerosol particles can activate and the median activation fraction is 0.89. In the case of a polluted environment ($N_a = 1000$ cm^{-3}), relatively few aerosol particles activate without SGS variability (median number fraction of 0.10). However, the activated fraction is significantly increased (median of 0.54) when SGS variability is considered. The representation of SGS velocities obviously changes the fraction of activated CCN. Including this effect in the UM should then enhance cloud droplet number concentrations (CDNC) and inhibit drizzle. This could potentially affect the precipitation patterns, evolution of the boundary layer, and the microphysical and macrophysical properties of the stratocumulus clouds. However, due to the myriad of feedbacks and competing effects occurring in boundary layer, we cannot robustly conclude beyond this point. Further work which fully integrates our SGS velocity framework in the UM to perform interactive ACI experiments is thus required to quantify the relative importance of SGS updraft velocity at kilometer scale.

7. Summary and Outlook

In this study, we have presented a computationally efficient framework to address the problem of subgrid-scale (SGS) updraft velocity in mesoscale models with kilometer-scale grid resolution or less. The treatment of SGS vertical velocity is important because updraft velocities strongly control the activation of aerosols. To understand the partitioning of resolved and unresolved velocities at kilometer scales, we used LES and high-resolution aircraft observations of marine stratocumulus and trade wind cumulus clouds to develop a scale-linking partition function of the total updraft velocity variability. This is inspired by the work of *Honnert et al.* [2011] but extended to represent two types of moist boundary layers. The resolved vertical velocity variability from the large-scale model is then corrected using the partition function to account for the missing SGS component. Our method assumes that the NWP model can resolve some of the cloud-scale vertical velocity variability, limiting this approach to grid sizes smaller than ~2 km. Once the total variability is assessed in the large-scale model, it could be used do define an assumed probability density function of vertical velocities or to derive a characteristic velocity for use in the aerosol activation calculation [e.g., *Golaz et al.*, 2011; *West et al.*, 2013]. In contrast to previous large-scale studies, our method does not rely on a turbulent kinetic energy diagnostic or a high-order turbulence scheme as a proxy for the vertical velocity variability. Thus, unlike diagnosed TKE based parametrization [e.g., *Golaz et al.*, 2011; *West et al.*, 2013], this framework has the potential to work with convective parametrization, in which TKE is not diagnosed.

We have tested our developments using forecasts of a marine stratocumulus and a cold air outbreak case performed with the United Kingdom Met Office Unified Model (UM). These forecasts use model grid resolution ranging from 100 m to 1 km. We show that without correction, the variability of updraft velocity decreases with decreasing model resolution. Applying our parametrization leads to consistent estimates of vertical velocity variability across the different resolutions. The 1 km UM model results have been compared with reference LES and aircraft measurements. In the stratocumulus simulations, the averaged cloud base standard deviation of w, σ_w, is between 0.04 and 0.05 m s^{-1}. Once the SGS variability is considered, the new estimates of σ_w are between 0.343 and 0.441 m s^{-1}. This compares well with LES and aircraft estimates of, respectively, 0.38 and 0.54 m s^{-1}. The inclusion of the SGS term in these simulations corresponds to an increase of a factor ~8.1 of the resolved term. In agreement with *Tonttila et al.* [2011], it shows that the SGS variability of w is still dominant at grid resolution of 1 km, and therefore, it is important to adequately constrain this term in the frame of aerosol-cloud interaction studies. Similarly, the 1 km model for the cold air outbreak provides satisfactory new estimates of σ_w with an averaged value of 0.45 m s^{-1} (0.86 m s^{-1}) in the stratiform (convective) area of the simulation domain compared to the value of 0.54 m s^{-1} (0.87 m s^{-1}) in the LES results. The relative increases here is a factor of ~4.8 which is smaller than in the previous case but still predominant. These latter results are encouraging because the cold air outbreak simulations involve a different cloud microphysics and a different large-scale environment to in the case studies analyzed to construct our framework and suggests some robustness in our methodology. More types of boundary layers and cloud environments should be modeled to validate the apparent robustness of this framework.

To understand the importance of this change in σ_w, we ran simple sensitivity experiments using the *Shipway and Abel* [2010] activation scheme to perform off-line calculations of the cloud condensation nuclei (CCN) activated fraction. The estimates of σ_w from the 1 km model results of the stratocumulus case were used as inputs. Our results suggest that by including the SGS contribution, an increases in CCN-activated fraction, from 0.52 to 0.89 (respectively, 0.10 to 0.54) for a clean (respectively, polluted) aerosol environment, could

occur. This result highlights the importance of using SGS information to correct vertical velocities for aerosol activation in kilometer-scale simulations.

Future work will first consist of implementing these developments within the UM in order to investigate the impacts on cloud droplet number concentrations (CDNC) and radiative flux perturbations. These developments will be tested jointly with the new UM cloud microphysics packages [see *Shipway and Hill*, 2012, appendix] and will provide motivation for future interactive aerosol-cloud interaction simulations in a high-resolution NWP suite.

It is known that kilometer-scale models have difficulties reproducing the correct aerosol activation behavior due to an underestimate of vertical velocity [e.g., *Ivanova and Leighton*, 2008]. The main focus of this study was to improve the vertical velocity variance derived from kilometer-scale models and hence improve the representation of aerosol activation. With the continuous increase in computational power, it is likely that global cloud-resolving models or cloud-resolving models (CRM) embedded within each grid cell of a global model, the so-called Multiscale Modeling Framework (MMF) [*Randall et al.*, 2003], will improve their resolution, until the grey zone becomes an issue for those models as well as NWP. Currently, CRMs used in MMFs operate at typical resolution of 2–4 km. This produces reasonable simulations for deep convection but shallow convective processes and turbulence still need to be parameterized. The resolution of these embedded CRMs will likely increase in the future (e.g., to represent boundary layer clouds such as stratocumulus clouds which always pose challenges in GCMs), to fully take advantage of the MMF approach. The method proposed here will then be relevant for CRMs with resolution finer than ~2 km.

Appendix A: Unified Model Nested Simulations

The UM is used to produce a first series of one-way nested simulations at increasing resolution (~40 km, 12 km, 4 km, and 1 km). The data used in the results (section 5) are from nested 1 km horizontal resolution model based on a modified operational UM-UKV configuration. In the vertical, there are 70 levels stretching up to 40 km (52 below 10 km, 33 below 4 km, and 16 below 1 km). The limited area domains use a rotated-pole coordinate system, placing the equator at the center of the domain allowing an approximately uniform grid. The driving model is the Global Atmosphere 3.0 configuration of the UM [*Walters et al.*, 2011]. The resolution used is N320 (0.5625° in longitude by 0.375° in latitude) with 70 vertical levels below 80 km, quadratically spaced to give more levels near the surface. Lateral boundary conditions are updated at 1 h intervals to the 12 and 4 km nests and at 30 min intervals to the 1 km nest. The first 12 km nested domain is reconfigured from the global model at $T + 1$ h and thereafter is free running throughout the case study periods, forced only at the boundaries by the global model. The second nested domain has a horizontal grid length of 4 km. Finally, a 1 km horizontal grid length inner domain is reconfigured at $T + 1$ h from the 4 km domain (i.e., $T + 3$ h from the global model) and is free running, forced at the boundaries by the 4 km model. There is no convection scheme in the 4 and 1 km grid-scale models, so convection is handled explicitly at the grid scale. The model is nonhydrostatic and uses a semi-Lagrangian dynamical formulation [*Cullen et al.*, 1997; *Davies et al.*, 2005]. More details on the Unified Model can be found in *Walters et al.* [2011].

The second cascade of nested high-resolution simulations (UM-HIRES-VOCALS and UM-HIRES-CONSTRAIN) are performed using the 1 km models as reference boundary conditions. The inner domains use horizontal spacings of 333 m and 100 m for the UM-HIRES-VOCALS runs (initialized at $T + 1$ h and $T + 2$ h from the 1 km model) and 500 m, 200 m, and 100 m for the UM-HIRES-CONSTRAIN (respectively, $T + 1$ h, $T + 2$ h, and $T + 3$ h from 1 km model). The 333 m and 100 m UM-HIRES-VOCALS domains are 500 by 500 grid points on the horizontal centered on 76°W, 20°S, whereas the 500 m, 200 m, and 100 m UM-HIRES-CONSTRAIN domains are, respectively, 400 by 900, 630 by 1100, and 720 by 1110 grid points on the horizontal and located approximately north of the Isle of Lewis (58.1°N, 6.2°W) in the "convective area" of the 1 km model. The boundaries of the inner high-resolution domains are overlaid on the respective 1 km host domains in Figure 7. UM-HIRES-VOCALS and UM-HIRES-CONSTRAIN use the same vertical grid spacing as the 1 km model.

Acknowledgments
This work was funded by the Natural Environment Research Council (NERC) Aerosol-Cloud Interactions—a Directed Programme to Reduce Uncertainty in Forcing (ACID-PRUF) programme, grant code NE/I020121/1. The authors thank the scientists, ground crew and aircrew of the FAAM BAe-146 and C-130 aircraft, who were instrumental in the collection of the data analyzed from the VOCALS-REx campaign. The C-130 data were provided by NCAR/EOL, under sponsorship of the National Science Foundation. http://data.eol.ucar.edu/. The FAAM BAe-146 is jointly funded by the UK Met Office and the Natural Environment Research Council. VOCALS was supported by the UK Met Office and NERC, the latter through grant NE/F019874/1. We gratefully thank the Editor S. Ghan and the anonymous reviewers for useful comments that helped us to improve the manuscript.

References

Abel, S. J., and I. A. Boutle (2012), An improved representation of the raindrop size distribution for single-moment microphysics schemes, *Q. J. R. Meteorolog. Soc.*, *138*(669), 2151–2162, doi:10.1002/qj.1949.

Abel, S. J., and B. J. Shipway (2007), A comparison of cloud-resolving model simulations of trade wind cumulus with aircraft observations taken during RICO, *Q. J. R. Meteorolog. Soc.*, *133*(624), 781–794, doi:10.1002/qj.55.

Ackerman, A. S., M. P. Kirkpatrick, D. E. Stevens, and O. B. Toon (2004), The impact of humidity above stratiform clouds on indirect aerosol climate forcing, *Nature*, *432*, 1014–1017, doi:10.1038/nature03174.

Albrecht, B. A., C. S. Bretherton, D. Johnson, W. H. Scubert, and A. S. Frisch (1995), The atlantic stratocumulus transition experiment-ASTEX, *Bull. Am. Meteorol. Soc.*, *76*, 889–904, doi:10.1175/1520-0477(1995)076<0889:TASTE>2.0.CO;2.

Boutle, I. A., and S. J. Abel (2012), Microphysical controls on the stratocumulus topped boundary-layer structure during VOCALS-REx, *Atmos. Chem. Phys.*, *12*(6), 2849–2863, doi:10.5194/acp-12-2849-2012.

Bretherton, C. S., R. Wood, R. C. George, D. Leon, G. Allen, and X. Zheng (2010), Southeast Pacific stratocumulus clouds, precipitation and boundary layer structure sampled along 20s during VOCALS-REx, *Atmos. Chem. Phys.*, *10*(21), 10,639–10,654, doi:10.5194/acp-10-10639-2010.

Brown, A., S. Milton, M. Cullen, B. Golding, J. Mitchell, and A. Shelly (2012), Unified modeling and prediction of weather and climate: A 25-year journey, *Bull. Am. Meteorol. Soc.*, *93*, 1865–1877, doi:10.1175/BAMS-D-12-00018.1.

Connolly, P. J., G. Vaughan, P. Cook, G. Allen, H. Coe, T. W. Choularton, C. Dearden, and A. Hill (2013), Modelling the effects of gravity waves on stratocumulus clouds observed during VOCALS-UK, *Atmos. Chem. Phys.*, *13*(14), 7133–7152, doi:10.5194/acp-13-7133-2013.

Cullen, M. J., T. Davies, M. H. Mawson, J. A. James, S. C. Coulter, and A. Malcolm (1997), An overview of numerical methods for the next generation U.K. NWP and climate model, in *Numerical Methods in Atmospheric and Ocean Modelling: The Andre J. Robert Memorial*, vol. 35, edited by C. A. Lin, R. Laprise, and H. Ritchie, pp. 425–444, Canadian Meteorol. Oceanogr. Soc., Ottawa, Canada, doi:10.1080/070559001997.9687359.

Davies, T., M. J. P. Cullen, A. J. Malcolm, M. H. Mawson, A. Staniforth, A. A. White, and N. Wood (2005), A new dynamical core for the met office's global and regional modelling of the atmosphere, *Q. J. R. Meteorolog. Soc.*, *131*(608), 1759–1782, doi:10.1256/qj.04.101.

de Roode, S. R., and P. G. Duynkerke (1997), Observed Lagrangian transition of stratocumulus into cumulus during ASTEX: Mean state and turbulence structure, *J. Atmos. Sci.*, *54*(17), 2157–2173, doi:10.1175/1520-0469(1997)054<2157:OLTOSI>2.0.CO;2.

de Roode, S. R., P. G. Duynkerke, and H. J. J. Jonker (2004), Large-eddy simulation: How large is large enough?, *J. Atmos. Sci.*, *61*, 403–421, doi:10.1175/1520-0469(2004)061<0403:LSHLIL>2.0.CO;2.

Dorrestijn, J., D. T. Crommelin, A. P. Siebesma, and H. J. J. Jonker (2013), Stochastic parameterization of shallow cumulus convection estimated from high-resolution model data, *Theor. Comput. Fluid Dyn.*, *27*, 133–148, doi:10.1007/s00162-012-0281-y.

Field, P. R., R. J. Cotton, K. McBeath, A. P. Lock, S. Webster, and R. P. Allan (2013), Improving a convection-permitting model simulation of a cold air outbreak, *Q. J. R. Meteorolog. Soc.*, *40*, 124–138, doi:10.1002/qj.2116.

Forster, P., et al. (2007), Changes in atmospheric constituents and in radiative forcing, in *Climate Change 2007: The Physical Science Basis. Contribution of Working Group I to the Fourth Assessment Report of the Intergovernmental Panel on Climate Change*, edited by S. Soloman et al., pp. 129–234, Cambridge Univ. Press, Cambridge, U. K.

Ghan, S. J., L. R. Leung, R. C. Easter, and H. Abdul-Razzak (1997), Prediction of cloud droplet number in a general circulation model, *J. Geophys. Res.*, *102*(D18), 21,777–21,794, doi:10.1029/97JD01810.

Ghan, S. J., H. Abdul-Razzak, A. Nenes, Y. Ming, X. Liu, M. Ovchinnikov, B. Shipway, N. Meskhidze, J. Xu, and X. Shi (2011), Droplet nucleation: Physically-based parameterizations and comparative evaluation, *J. Adv. Model. Earth Syst.*, *3*, M10001, doi:10.1029/2011MS000074.

Golaz, J.-C., V. E. Larson, and W. R. Cotton (2002), A pdf-based model for boundary layer clouds. Part I: Method and model description, *J. Atmos. Sci.*, *59*, 3540–3551, doi:10.1175/1520-0469(2002)059<3540:APBMFB>2.0.CO;2.

Golaz, J.-C., M. Salzmann, L. J. Donner, L. W. Horowitz, Y. Ming, and M. Zhao (2011), Sensitivity of the aerosol indirect effect to subgrid variability in the cloud parameterization of the GFDL atmosphere general circulation model AM3, *J. Clim.*, *24*, 3145–3160, doi:10.1175/2010JCLI3945.1.

Grabowski, W. W., and H. Morrison (2011), Indirect impact of atmospheric aerosols in idealized simulations of convective-radiative quasi equilibrium. Part II: Double-moment microphysics, *J. Clim.*, *24*, 1897–1912, doi:10.1175/2010JCLI3647.1.

Guibert, S., J. R. Snider, and J.-L. Brenguier (2003), Aerosol activation in marine stratocumulus clouds: 1. Measurement validation for a closure study, *J. Geophys. Res.*, *108*, 8628, doi:10.1029/2002JD002678.

Guo, H., J.-C. Golaz, L. J. Donner, V. E. Larson, D. P. Schanen, and B. M. Griffin (2010), Multi-variate probability density functions with dynamics for cloud droplet activation in large-scale models: Single column tests, *Geosci. Model Dev.*, *3*, 475–486, doi:10.5194/gmd-3-475-2010.

Hill, A. A., S. Dobbie, and Y. Yin (2008), The impact of aerosols on non-precipitating marine stratocumulus. I: Model description and prediction of the indirect effect, *Q. J. R. Meteorolog. Soc.*, *134*(634), 1143–1154, doi:10.1002/qj.278.

Hogan, R. J., A. L. M. Grant, A. J. Illingworth, G. N. Pearson, and E. J. O'Connor (2009), Vertical velocity variance and skewness in clear and cloud-topped boundary layers as revealed by doppler lidar, *Q. J. R. Meteorolog. Soc.*, *135*(640), 635–643, doi:10.1002/qj.413.

Honnert, R., V. Masson, and F. Couvreux (2011), A diagnostic for evaluating the representation of turbulence in atmospheric models at the kilometric scale, *J. Atmos. Sci.*, *68*, 3112–3131, doi:10.1175/JAS-D-11-061.1.

Ivanova, I. T., and H. G. Leighton (2008), Aerosol-cloud interactions in a Mesoscale Model. Part I: Sensitivity to activation and collision-coalescence, *J. Atmos. Sci.*, *65*(2), 289–308, doi:10.1175/2007JAS2207.1.

Jiang, H., and G. Feingold (2006), Effect of aerosol on warm convective clouds: Aerosol-cloud-surface flux feedbacks in a new coupled large eddy model, *J. Geophys. Res.*, *111*, D01202, doi:10.1029/2005JD006138.

Jones, C. R., C. S. Bretherton, and D. Leon (2011), Coupled vs. decoupled boundary layers in VOCALS-REx, *Atmos. Chem. Phys.*, *11*(14), 7143–7153, doi:10.5194/acp-11-7143-2011.

Khairoutdinov, M., and Y. Kogan (2000), A new cloud physics parameterization in a large-eddy simulation model of marine stratocumulus, *Mon. Weather Rev.*, *128*, 229–243, doi:10.1175/1520-0493(2000)128<0229:ANCPPI>2.0.CO;2.

Kocha, C., J.-P. Lafore, P. Tulet, and Y. Seity (2012), High-resolution simulation of a major west african dust-storm: Comparison with observations and investigation of dust impact, *Q. J. R. Meteorolog. Soc.*, *138*(663), 455–470, doi:10.1002/qj.927.

Koren, I., and G. Feingold (2011), Aerosol-cloud-precipitation system as a predator-prey problem, *Proc. Natl. Acad. Sci.*, *108*, 12,227–12,232, doi:10.1073/pnas.1101777108.

Larson, V. E., J. Golaz, and W. R. Cotton (2002), Small-Scale and mesoscale variability in cloudy boundary layers: Joint probability density functions, *J. Atmos. Sci.*, *59*(24), 3519–3539, doi:10.1175/1520-0469(2002)059<3519:SSAMVI>2.0.CO;2.

Lock, A. P. (2011), The parametrization of boundary-layer processes, in Unified Model Documentation Paper 24, Met Office, Exeter, U. K. [Available at http://collab.metoffice.gov.uk/twiki/pub/Support/Umdp/024_79.pdf.]
Lock, A. P., A. R. Brown, M. R. Bush, G. M. Martin, and R. N. B. Smith (2000), A new boundary layer mixing scheme. Part I: Scheme description and single-column model tests, *Mon. Weather Rev.*, *128*, 3187–3199, doi:10.1175/1520-0493(2000)128<3187:ANBLMS>2.0.CO;2.
Lohmann, U., and J. Feichter (2005), Global indirect aerosol effects: A review, *Atmos. Chem. Phys.*, *5*(3), 715–737, doi:10.5194/acp-5-715-2005.
Lohmann, U., J. Feichter, C. C. Chuang, and J. E. Penner (1999), Prediction of the number of cloud droplets in the ECHAM GCM, *J. Geophys. Res.*, *104*, 9169–9198.
Lu, M.-L., W. C. Conant, H. H. Jonsson, V. Varutbangkul, R. C. Flagan, and J. H. Seinfeld (2007), The Marine Stratus/Stratocumulus Experiment (MASE): Aerosol-cloud relationships in marine stratocumulus, *J. Geophys. Res.*, *112*, D10209, doi:10.1029/2006JD007985.
Marshall, J. S., and W. M. K. Palmer (1948), The distribution of raindrops with size, *.J. Metrol.*, *5*(4), 165–166, doi:10.1175/1520-0469(1948)005<0165:TDORWS>2.0.CO;2.
McBeath, K., P. R. Field, and R. J. Cotton (2013), Using operational weather radar to assess high-resolution numerical weather prediction over the British Isles for a cold air outbreak case-study, *Q. J. R. Meteorolog. Soc.*, *140*, 225–239, doi:10.1002/qj.2123.
Ming, Y., V. Ramaswamy, L. J. Donner, V. T. J. Phillips, S. A. Klein, P. A. Ginoux, and L. W. Horowitz (2007), Modeling the interactions between aerosols and liquid water clouds with a self-consistent cloud scheme in a general circulation model, *J. Atmos. Sci.*, *64*(4), 1189–1209, doi:10.1175/JAS3874.1.
Morales, R., and A. Nenes (2010), Characteristic updrafts for computing distribution-averaged cloud droplet number and stratocumulus cloud properties, *J. Geophys. Res.*, *115*, D18220, doi:10.1029/2009JD013233.
Morrison, H., and A. Gettelman (2008), A new two-moment bulk stratiform cloud microphysics scheme in the community atmosphere model, version 3 (CAM3). Part I: Description and numerical tests, *J. Clim.*, *21*, 3642–3659.
Morrison, H., and J. O. Pinto (2005), Mesoscale modeling of springtime arctic mixed-phase stratiform clouds using a new two-moment bulk microphysics scheme, *J. Atmos. Sci.*, *62*(10), 3683–3704, doi:10.1175/JAS3564.1.
Peng, Y., U. Lohmann, and R. Leaitch (2005), Importance of vertical velocity variations in the cloud droplet nucleation process of marine stratus clouds, *J. Geophys. Res.*, *110*(D21), D21213, doi:10.1029/2004JD004922.
Petch, J. C. (2006), Sensitivity studies of developing convection in a cloud-resolving model, *Q. J. R. Meteorolog. Soc.*, *132*(615), 345–358, doi:10.1256/qj.05.71.
Pruppacher, H. R., and J. D. Klett (1997), *Microphysics of Clouds and Precipitation*, 954 pp., Kluwer Acad., Dordrecht, The Netherlands.
Randall, D. A., M. Khairoutdinov, A. Arakawa, and W. Grabowski (2003), Breaking the cloud-parameterization deadlock, *Bull. Am. Meteorol. Soc.*, *84*, 1547–1564, doi:10.1175/BAMS-84-11-1547.
Rauber, R. M., et al. (2007), Rain in shallow cumulus over the ocean: The RICO campaign, *Bull. Am. Meteorol. Soc.*, *88*, 1912–1928, doi:10.1175/BAMS-88-12-1912.
Ricard, D., C. Lac, S. Riette, R. Legrand, and A. Mary (2012), Kinetic energy spectra characteristics of two convection-permitting limited-area models AROME and Meso-NH, *Q. J. R. Meteorolog. Soc.*, *139*, 1327–1341, doi:10.1002/qj.2025.
Sandu, I., J. L. Brenguier, O. Geoffroy, O. Thouron, and V. Masson (2008), Aerosol impacts on the diurnal cycle of marine stratocumulus, *J. Atmos. Sci.*, *65*, 2705–2718, doi:10.1175/2008JAS2451.1.
Seifert, A., C. Köhler, and K. D. Beheng (2012), Aerosol-cloud-precipitation effects over germany as simulated by a convective-scale numerical weather prediction model, *Atmos. Chem. Phys.*, *12*(2), 709–725, doi:10.5194/acp-12-709-2012.
Shipway, B. J., and S. J. Abel (2010), Analytical estimation of cloud droplet nucleation based on an underlying aerosol population, *Atmos. Res.*, *96*, 344–355, doi:10.1016/j.atmosres.2009.10.005.
Shipway, B. J., and A. A. Hill (2012), Diagnosis of systematic differences between multiple parametrizations of warm rain microphysics using a kinematic framework, *Q. J. R. Meteorolog. Soc.*, *138*(669), 2196–2211, doi:10.1002/qj.1913.
Shutts, G. J., and T. N. Palmer (2007), Convective forcing fluctuations in a cloud-resolving model: Relevance to the stochastic parameterization problem, *J. Clim.*, *20*(2), 187–202, doi:10.1175/JCLI3954.1.
Skamarock, W. C. (2004), Evaluating mesoscale NWP models using kinetic energy spectra, *Mon. Weather Rev.*, *132*(12), 3019–3032, doi:10.1175/MWR2830.1.
Smagorinsky, J. (1963), General circulation experiments with the primitive equations, *Mon. Weather Rev.*, *91*(3), 99–164, doi:10.1175/1520-0493(1963)091<0099:GCEWTP>2.3.CO;2.
Smith, R. N. B. (1990), A scheme for predicting layer clouds and their water content in a general circulation model, *Q. J. R. Meteorolog. Soc.*, *116*(492), 435–460, doi:10.1002/qj.49711649210.
Stevens, B., and O. Boucher (2012), Climate science: The aerosol effect, *Nature*, *490*, 40–41, doi:10.1038/490040a.
Stevens, B., and G. Feingold (2009), Untangling aerosol effects on clouds and precipitation in a buffered system, *Nature*, *461*, 607–613, doi:10.1038/nature08281.
Tonttila, J., E. J. O'Connor, S. Niemelä, P. Räisänen, and H. Järvinen (2011), Cloud base vertical velocity statistics: A comparison between an atmospheric mesoscale model and remote sensing observations, *Atmos. Chem. Phys.*, *11*(17), 9207–9218, doi:10.5194/acp-11-9207-2011.
Tonttila, J., P. Räisänen, and H. Järvinen (2013), Monte carlo-based subgrid parameterization of vertical velocity and stratiform cloud microphysics in ECHAM5.5-HAM2, *Atmos. Chem. Phys.*, *13*(15), 7551–7565, doi:10.5194/acp-13-7551-2013.
Tripoli, G. J., and W. R. Cotton (1980), A numerical investigation of several factors contributing to the observed variable intensity of deep convection over south Florida, *J. Appl. Meteorol.*, *19*(9), 1037–1063, doi:10.1175/1520-0450(1980)019<1037:ANIOSF>2.0.CO;2.
Twomey, S. (1959), The nuclei of natural cloud formation: Part II. The supersaturation in natural clouds and the variation of cloud droplet concentration, *Geof. Pura Appl.*, *43*(1), 243–249, doi:10.1007/BF01993560.
van der Dussen, J. J., S. R. de Roode, A. S. Ackerman, P. N. Blossey, C. S. Bretherton, M. J. Kurowski, A. P. Lock, R. A. J. Neggers, I. Sandu, and A. P. Siebesma (2013), The GASS/EUCLIPSE model intercomparison of the stratocumulus transition as observed during ASTEX: LES results, *J. Adv. Model. Earth Syst.*, *5*, 483–499, doi:10.1002/jame.20033.
Walters, D. N., et al. (2011), The Met Office Unified Model Global Atmosphere 3.0/3.1 and JULES Global Land 3.0/3.1 configurations, *Geosci. Model Dev.*, *4*(4), 919–941, doi:10.5194/gmd-4-919-2011.
Wang, M., S. Ghan, M. Ovchinnikov, X. Liu, R. Easter, E. Kassianov, Y. Qian, and H. Morrison (2011), Aerosol indirect effects in a multi-scale aerosol-climate model PNNL-MMF, *Atmos. Chem. Phys.*, *11*(11), 5431–5455, doi:10.5194/acp-11-5431-2011.
West, R. E. L., P. Stier, A. Jones, C. E. Johnson, G. W. Mann, N. Bellouin, and Z. Kipling (2013), The importance of vertical velocity variability for estimates of the indirect aerosol effects, *Atmos. Chem. Phys. Discuss.*, *13*(10), 27,053–27,113, doi:10.5194/acpd-13-27053-2013.
Wilkinson, J. (2011), The large-scale precipitation parametrization scheme, in Unified Model Documentation Paper 24, Met Office, Exeter, U. K. [Available at http://collab.metoffice.gov.uk/twiki/pub/Support/Umdp/026_77.pdf.]

Wilson, D. R., and S. P. Ballard (1999), A microphysically based precipitation scheme for the UK meteorological office unified model, *Q. J. R. Meteorolog. Soc.*, *125*(557), 1607–1636, doi:10.1002/qj.49712555707.

Wood, R., et al. (2011), The VAMOS ocean-cloud-atmosphere-land study regional experiment (VOCALS-REx): Goals, platforms, and field operations, *Atmos. Chem. Phys.*, *11*(2), 627–654, doi:10.5194/acp-11-627-2011.

Wyngaard, J. C. (2004), Toward numerical modeling in the terra incognita, *J. Atmos. Sci.*, *61*, 1816–1826, doi:10.1175/1520-0469(2004)061<1816:TNMITT>2.0.CO;2.

Xue, H., and G. Feingold (2006), Large-eddy simulations of trade wind cumuli: Investigation of aerosol indirect effects, *J. Atmos. Sci.*, *63*, 1605–1622, doi:10.1175/JAS3706.1.

Zhu, P., and W. Zhao (2008), Parameterization of continental boundary layer clouds, *J. Geophys. Res.*, *113*(D10), D10201, doi:10.1029/2007JD009315.

Zhu, P., and P. Zuidema (2009), On the use of pdf schemes to parameterize sub-grid clouds, *Geophys. Res. Lett.*, *36*, L05807, doi:10.1029/2008GL036817.